

DTIC FILE COPY

4

GL-TR-90-0025

Propagation of Regional Phases in the Basin and Range

K. Priestley

University of Nevada, Reno  
Seismological Laboratory  
Reno, NV 89557-0141

2 February 1990

Final Report  
1 January 1987-30 September 1989

APPROVED FOR PUBLIC RELEASE; DISTRIBUTION UNLIMITED

DTIC  
ELECTE  
JUL 31 1990  
E

GEOPHYSICS LABORATORY  
AIR FORCE SYSTEMS COMMAND  
UNITED STATES AIR FORCE  
HANSCOM AIR FORCE BASE, MASSACHUSETTS 01731-5000

AD-A224 862


90 07 00 104


SPONSORED BY  
Defense Advanced Research Projects Agency  
Nuclear Monitoring Research Office  
ARPA ORDER NO 5299

MONITORED BY  
Geophysics Laboratory  
F19628-87-K-0009

The views and conclusions contained in this document are those of the authors and should not be interpreted as representing the official policies, either expressed or implied, of the Defense Advanced Research Projects Agency or the U.S. Government.

This technical report has been reviewed and is approved for publication.

  
JAMES F. LEWKOWICZ  
Contract Manager  
Solid Earth Geophysics Branch  
Earth Sciences Division

  
JAMES F. LEWKOWICZ  
Branch Chief  
Solid Earth Geophysics Branch  
Earth Sciences Division

FOR THE COMMANDER

  
DONALD H. ECKHARDT, Director  
Earth Sciences Division

This report has been reviewed by the ESD Public Affairs Office (PA) and is releasable to the National Technical Information Service (NTIS).

Qualified requestors may obtain additional copies from the Defense Technical Information Center. All others should apply to the National Technical Information Service.

If your address has changed, or if you wish to be removed from the mailing list, or if the addressee is no longer employed by your organization, please notify GL/IMA, Hanscom AFB, MA 01731-5000. This will assist us in maintaining a current mailing list.

Do not return copies of this report unless contractual obligations or notices on a specific document requires that it be returned.

REPORT DOCUMENTATION PAGE				Form Approved OMB No. 0704-0188	
1a. REPORT SECURITY CLASSIFICATION Unclassified			1b. RESTRICTIVE MARKINGS		
2a. SECURITY CLASSIFICATION AUTHORITY			3. DISTRIBUTION / AVAILABILITY OF REPORT Approved for public release; distribution unlimited		
2b. DECLASSIFICATION / DOWNGRADING SCHEDULE					
4. PERFORMING ORGANIZATION REPORT NUMBER(S) n/a			5. MONITORING ORGANIZATION REPORT NUMBER(S) GL-TR-90-0025		
6a. NAME OF PERFORMING ORGANIZATION Seismological Lab		6b. OFFICE SYMBOL (if applicable)	7a. NAME OF MONITORING ORGANIZATION Geophysical Laboratory		
6c. ADDRESS (City, State, and ZIP Code) University of Nevada, Reno Reno, NV 89557-0141			7b. ADDRESS (City, State, and ZIP Code) Hanscom Air Force Base Massachusetts 01731-5000		
8a. NAME OF FUNDING / SPONSORING ORGANIZATION Defence Advanced Research Projects Agency		8b. OFFICE SYMBOL (if applicable) NMRO	9. PROCUREMENT INSTRUMENT IDENTIFICATION NUMBER F19628-87-K-0009		
8c. ADDRESS (City, State, and ZIP Code) 1400 Wilson Blvd. Arlington, VA 22209			10. SOURCE OF FUNDING NUMBERS		
			PROGRAM ELEMENT NO. 61101E	PROJECT NO. 7A10	TASK NO. DA
11. TITLE (Include Security Classification) Propagation of Regional Phases in the Basin and Range					
12. PERSONAL AUTHOR(S) K. Priestley					
13a. TYPE OF REPORT Final		13b. TIME COVERED FROM 1/1/87 TO 9/30/89		14. DATE OF REPORT (Year, Month, Day) 1990, Feb. 2.	
15. PAGE COUNT 48					
16. SUPPLEMENTARY NOTATION					
17. COSATI CODES			18. SUBJECT TERMS (Continue on reverse if necessary and identify by block number) Regional seismic phases, Attenuation, Joint verification experiment, High frequency P-wave spectra, Crustal Structure, Eastern Kazakh.		
FIELD	GROUP	SUB-GROUP			
19. ABSTRACT (Continue on reverse if necessary and identify by block number)  <div style="text-align: center;">(Next Page)</div>					
20. DISTRIBUTION / AVAILABILITY OF ABSTRACT <input type="checkbox"/> UNCLASSIFIED/UNLIMITED <input type="checkbox"/> SAME AS RPT. <input type="checkbox"/> DTIC USERS			21. ABSTRACT SECURITY CLASSIFICATION Unclassified		
22a. NAME OF RESPONSIBLE INDIVIDUAL James F. Lewkowicz			22b. TELEPHONE (Include Area Code) (617) 577-3222		22c. OFFICE SYMBOL GL/LWH

Measurement of the spatial decay of spectral amplitudes of the higher-mode seismic surface wave train  $L_g$  indicates that in the Great Basin, the apparent seismic quality factor,  $Q$ , is a function of frequency. Analysis of recordings from a NTS nuclear explosion made along a 300 km profile through northwest Nevada yield the function  $Q(f) = 206f^{0.68}$  over the band  $0.3 \leq f \leq 10.0$  Hz. Similar analysis using numerous recordings of earthquakes along paths which provide a good average sampling of the Great Basin crust gives  $Q(f) = 214(\pm 15)f^{0.54 \pm 0.09}$ , for  $0.3 \leq f \leq 5.0$  Hz. If the crustal sampling by  $L_g$  energy from nuclear explosions (surface sources) is primarily in the shallow crust, as has been suggested, then these results indicate a greater frequency dependence of apparent  $Q$  there than at depth. To better estimate the errors in  $Q$  at each frequency, we have used a moving window spectral analysis technique described by Butler et al (1987) to analysis the nuclear explosion profile data. Using this method we found the apparent attenuation for vertical component  $L_g$ , transverse component  $L_g$ , and vertical component  $P_g$  are  $Q(f) = 296f^{0.51}$ ,  $Q(f) = 202f^{0.57}$ , and  $Q(f) = 198f^{0.45}$  respectively, for the frequency band  $0.3 \leq f \leq 10.0$  Hz.

During August and September, 1988, the United States and the Soviet Union conducted a Joint Verification Experiment in which each country was permitted to observe a nuclear explosion at the other country's test site using hydrodynamic means. We have seismically recorded the Soviet Explosion at four stations at regional distance ( $\Delta \leq 750$  km). The peak-to-peak particle motion in the P-wave varied from  $7.54 \times 10^{-1}$  cm/sec at  $\approx 160$  km to  $1.02 \times 10^{-2}$  cm/sec at  $\Delta \approx 740$  km. The average  $m_b(L_g)$  was 5.97 corresponding to a yield of 120 KT, based on the NTS  $m_b(L_g)$  - yield relation of Patton [1988]. The average  $P_n$  corner frequency of the Soviet explosion was 4 Hz with evidence of a second corner at about 0.7 Hz. Both of these corners could be the effect of spall. Near-regional seismograms of the Soviet JVE explosion show a large arrival within the  $L_g$  phase on the transverse component at all four sites. This may correspond to tectonic release accompanying the explosion, or to the effects of anisotropy on seismic wave propagation.

Observations of 10-, 20-, and 30-Hz P-wave spectral amplitudes from earthquakes and explosions are compared with the Archambeau [1968, 1972] earthquake model featuring a P-wave falloff of  $\omega^{-3}$  beyond the corner frequency, a modified Brune [1970, 1971] earthquake model with  $\omega^{-2}$  falloff, and the Sharpe [1942] explosion model which has a  $\omega^{-2}$  falloff. The Archambeau and Sharpe models have been, in part, the basis of a proposal by Evernden et al [1986] that high-frequency ( $\approx 30$  Hz) seismic energy could provide an effective solution to the problem of detection and identification of low-yield coupled and fully decoupled underground nuclear explosions. The observations of earthquakes show an increase in spectral amplitude with moment approximately in agreement with the  $\omega^{-2}$  falloff model, and for larger moments, in disagreement with the  $\omega^{-3}$  model. Comparison of theoretical and actual seismograms narrow-band filtered at 30-Hz shows that in part the increase in spectral amplitude of earthquakes is due to the complex and long duration of the rupture process and not because of an increase in an impulsive first arrival like that characteristic of an explosion. The 30-Hz amplitudes for explosions show much scatter, and many events have a spectral falloff greater than the predicted by the Sharpe model. Whether this is due entirely to attenuation or is the actual source spectrum is not determined. High stress drop earthquakes are predicted to have larger spectral amplitudes than the Sharpe model. Thus any discrimination technique using high-frequency P-wave spectra should probably take into account differences in pulse shape and amplitude in the time domain.

Broadband receiver functions determined from teleseismic P waveforms at two seismic stations in eastern Kazakh, U.S.S.R., were inverted for the vertical velocity structure beneath the stations. The detailed broadband receiver functions are obtained by stacking source-equalized radial components of teleseismic P-waveforms. A time-domain inversion of the radial receiver function is used to determine the structure assuming a crustal model parameterized by flat-lying, homogeneous layers. The general features of the inversion results are: a complex shallow crust, velocities less than 6 km/s in the upper crust, a high velocity (6.9-7.5 km/s) lower crust, and a Moho that varies between 47 and 57 km depth. These results compare favorably with a composite velocity model from Deep Seismic Sounding data, but show lower velocities in the upper crust, and higher velocities in the lower crust. The results indicate that the crust in this region is relatively uniform, however the nature and depth of the Moho changes significantly across the region. The receiver function inversion structure for the Kazakh sites is similar to a published receiver function structure for a site on the Canadian shield.

# CONTENTS

	<u>PAGE</u>
<b>ATTENUATION OF REGIONAL SEISMIC PHASES IN THE GREAT BASIN</b>	<b>1</b>
Introduction	1
Data	2
Analysis	3
Discussion	6
References Cited	6
<b>REGIONAL SEISMIC RECORDINGS OF THE SOVIET NUCLEAR EXPLOSION OF THE JOINT VERIFICATION EXPERIMENT</b>	<b>17</b>
Introduction	17
Seismic Instrumentation	17
Data	18
Preliminary Analysis	18
References	20
<b>OBSERVATIONS OF HIGH-FREQUENCY P WAVE EARTHQUAKE AND EXPLOSION SPECTRA COMPARED WITH <math>\omega^{-3}</math>, <math>\omega^{-2}</math>, AND SHARPE SOURCE MODELS</b>	<b>21</b>
<b>CRUSTAL STRUCTURE IN EASTERN KAZAKH, USSR FROM TELESEISMIC RECEIVER FUNCTIONS.</b>	<b>29</b>



Accession For	
NTIS GRA&I	<input checked="" type="checkbox"/>
DTIC TAB	<input type="checkbox"/>
Unannounced	<input type="checkbox"/>
Justification	
By	
Distribution/	
Availability Codes	
Dist	Avail and/or Special
A-1	

## Attenuation of Regional Seismic Phases in the Great Basin

David E. Chavez<sup>1</sup> and Keith F. Priestley  
Seismological Laboratory, Mackay School of Mines  
University of Nevada - Reno, Reno, Nevada 89557

### ABSTRACT

Measurement of the spatial decay of spectral amplitudes of the higher-mode seismic surface wave train  $L_g$  indicates that in the Great Basin, the apparent seismic quality factor,  $Q$ , is a function of frequency. Analysis of recordings from a NTS nuclear explosion made along a 300 km profile through northwest Nevada yield the function  $Q(f) = 206f^{0.66}$  over the band  $0.3 \leq f \leq 10.0$  Hz. Similar analysis using numerous recordings of earthquakes along paths which provide a good average sampling of the Great Basin crust gives  $Q(f) = 214(\pm 15)f^{0.54 \pm 0.09}$ , for  $0.3 \leq f \leq 5.0$  Hz. If the crustal sampling by  $L_g$  energy from nuclear explosions (surface sources) is primarily in the shallow crust, as has been suggested, then these results indicate a greater frequency dependence of apparent  $Q$  there than at depth. To better estimate the errors in  $Q$  at each frequency, we have used a moving window spectral analysis technique described by Butler et al (1987) to analysis the nuclear explosion profile data. Using this method we found the apparent attenuation for vertical component  $L_g$ , transverse component  $L_g$ , and vertical component  $P_g$  are  $Q(f) = 296f^{0.51}$ ,  $Q(f) = 202f^{0.57}$ , and  $Q(f) = 198f^{0.45}$  respectively, for the frequency band  $0.3 \leq f \leq 10.0$  Hz.

### INTRODUCTION

In the past 15 years, considerable efforts have been devoted to the understanding of regional seismic phases. The majority of this work has concentrated on understanding the propagation characteristics of the crustal phase  $L_g$ . Much less effort has been expended on the other prominent regional seismic phases  $P_n$ ,  $S_n$ ,  $P_g$ , and  $S_g$ . Knowledge of the attenuation characteristics of regional seismic phases is important for both earthquake source mechanism studies and for the discrimination and yield estimation of small nuclear explosions.  $L_g$  consists of a superposition of higher mode surface waves and because of its averaging properties in excitation and transmission, Nuttli (1986) has suggested that it can be used to accurately estimate the yield of nuclear explosions. However, as Nuttli

<sup>1</sup>Current address: Institute of Geophysics and Planetary Physics, Scripps Institution of Oceanography, University of California, San Diego, La Jolla, California 92093

has demonstrated, it is necessary to know the  $L_g$  attenuation to within 30% along the propagation path in order to estimate the yield to within 10%. Most  $L_g$  attenuation studies to date have concentrated on the frequency band below 2 to 3 Hz. High frequency seismic waves have taken on added importance recently because they may be more diagnostic as to different earthquake source models, and because of suggestions that they may improve the capability to distinguish earthquakes and small or decoupled nuclear explosions (Evernden et al, 1986). Only recently has data become available for investigating the attenuation of higher frequency regional seismic phases. In this study we examine the attenuation of the  $L_g$  propagating within the Great Basin of western North America. We then make preliminary steps towards understanding the attenuation of the  $P_g$  phase propagating in the same region.

Cheng and Mitchell (1981) examined the spectra of long-period  $L_g$  for three paths in the Basin and Range province and estimated a constant shear wave  $Q$  of 85. Singh and Herrmann (1983) measured the decay of coda waves in this same region, and modeled frequency dependent  $Q$  as

$$Q(f) = Q_0 f^n \quad (1)$$

where  $Q_0$  is the  $Q$  at 1 Hz. They found  $Q(f) = 250(\pm 50)f^{0.45(\pm 0.05)}$ , and were able to relate their coda  $Q$  values to the  $L_g$  spatial attenuation coefficients, concluding that the same mechanism was responsible for both coda decay and  $L_g$  attenuation. Singh and Herrmann's result agrees with that of Cheng and Mitchell if we take the latter's value of 85 to be the  $L_g$   $Q$  at 5 seconds period, the predominate period in their data. Peseckis and Pomeroy (1984) examined the  $L_g$  coda of several Nevada Test Site (NTS) explosions recorded at regional short period stations and found an average relationship of  $Q(f) = 264f^{0.3}$ . However, Nuttli (1986) examined a similar data set and obtained  $Q(f) = 139f^{0.6}$ .

All of the above studies used band limited, analogue data recorded by only a few stations and along a limited number of paths. Using broad band digital recordings of earthquakes along a variety of paths, as well as data from a profile recording of a nuclear explosion, we have attempted to refine the  $L_g$  attenuation model for the Great Basin, and measure  $P_g$  attenuation.

## Data

The data analyzed were acquire from two sources. The first data set consist of digital seismograms of 11 regional earthquakes in and around the Great Basin recorded at four broad-band seismograph stations operated by the Lawrence Livermore National Laboratory (LLNL). Figure 1 shows the locations of the earthquakes, seismic stations, and the travel paths between them. We selected earthquakes which were recorded by at least three of the four stations and which covered a large range in epicentral distance (i.e., no two stations were at a similar distance). As indicated by the figure, the travel paths used provide a good sampling of the Great Basin crust. The second data set examined consist of

digital recordings of a nuclear explosion detonated at NTS on 12/5/85. Prior to that event, fourteen temporary sites were instrumented along a profile covering the distance range 200 to 500 km, extending northwest from NTS (Fig. 1). A record section of the vertical component seismograms from the nuclear explosion is shown in Figure 2. The  $L_g$  windows analyzed are marked on each seismogram. The beginning of each window corresponds to a group speed of 3.7 km/sec, while the end corresponds to the arrival of the fundamental mode surface wave train  $R_g$ , typically at around 2.7 km/sec. The  $R_g$  arrival times were determined by examining a low-pass filtered version of the record section. The same criteria was used in determining the  $L_g$  windows in the earthquake data.

### Analysis

Chavez and Priestley(1986) determined frequency dependent attenuation for the vertical component  $L_g$  phase from these data. They modeled the observed log-log  $L_g$  spectra as

$$A(f, R) = \frac{S(f)}{R^{0.5}} \exp\left(\frac{-\pi f t}{Q(f)}\right) \quad (2)$$

where  $A(f, R)$  is the spectral amplitude observed at a distance  $R$ ,  $f$  is frequency,  $t$  is the travel time,  $S(f)$  is the source term, and  $Q$  is the quality factor. Since this model does not consider scattering or radiation pattern effects it provides a measure of the apparent rather than the intrinsic  $Q$ . Radiation pattern effects should be minimal, however, since  $L_g$  consists of a large number of rays sampling a major fraction of the focal sphere.  $L_g$  has been successfully modelled as surface wave (Knopoff et al, 1973; Panza and Calcagnille, 1975), so we have assumed that the frequency domain geometrical spreading scales with the square root of distance. Taking the logarithm (base 10) of both sides of (2) yields

$$\log_{10} A(f, R) + \log_{10} R^{0.5} = \log_{10} S(f) - \left| \frac{1.364 f}{Q(f)} \right| t \quad (3)$$

which is the equation for a straight line, with the source term as the intercept and the  $Q$  term controlling the slope. Fixing  $f$ , we know  $A$ ,  $R$ , and  $t$  for each of the stations and we solve for  $S$  and  $Q$  using least-squares. By looping over all frequencies we obtain the source and  $Q$  spectra.

Figure 3 is a plot of the  $Q(f)$  functions obtained. Light lines indicate results from the earthquake data, the heavy line is for the explosion data. Only those values whose associated linear correlation coefficient exceeds 0.5 are included. A least-squares fit to the explosion data in Figure 3 is

$$Q(f) = 206 f^{0.68} \quad 0.3 \leq f \leq 10.0 \text{ Hz} \quad (4)$$

while a weighted fit of the earthquake data gives

$$Q(f) = 214(\pm 15) f^{0.54(\pm 0.09)} \quad 0.3 \leq f \leq 5.0 \text{ Hz} \quad (5)$$



The latter function was obtained by fitting the average of the earthquake derived  $Q$  functions, weighted by the standard deviation at each frequency. We might expect the error bars for the explosion data to be no greater than those given in (5) for the earthquake data. If we assume that our signal to noise criteria was successful in removing random error from the spectral amplitudes, then the error bars may be considered as a measure of the lateral heterogeneity of the attenuation structure. The relatively small magnitude of these errors suggests that the apparent  $Q$  function varies little within the Great Basin.

The  $Q$  function obtained using the explosion data is slightly different from that based on the earthquake data. While the values of  $Q_0$  found for both data sets are essentially identical, the explosion data indicate a greater frequency dependence. As a consequence, the  $Q$  from the earthquake data are consistently lower than that from the explosion data for frequencies above 1 Hz.

One drawback in using the above method to measure  $Q$  is that it is difficult to estimate the error in  $Q$  at each frequency. In order to do so, we have reprocessed our data using a moving window spectral analysis technique described by Butler et al (1987). The data are windowed for many different group speeds using overlapping Gaussian functions whose widths are scaled by the epicentral distance in such a manner that the windows are identical with respect to group speed at each distance. The amplitude spectra for each window are then themselves Gaussian windowed at intervals of 0.25 Hz, and the windowed spectrum is integrated to yield amplitude as a function of group speed and frequency. Figure 4 is an example of results of this procedure. Representing seismic data in this manner provides a quantitative description of the frequency content of the signal as a function of time. The phases  $P_g$  and  $L_g$  are clearly visible as ridges in frequency-group speed space. The loss of high frequency energy in the coda is also apparent.

Once these data are corrected for geometrical spreading we can solve for  $Q$  as described above, only this time we obtain apparent attenuation as a function of group speed as well as frequency. The attenuation for a particular phase is determined by taking the average over the group speed window for that phase. The standard deviations obtained at each frequency are then a measure of the error in attenuation for that phase.

Before doing this type of analysis it is necessary to first address the question of the nature of geometrical spreading when using this technique.  $L_g$  is composed of higher mode surface waves which decay in the frequency domain as  $R^{0.5}$ . However, the moving window spectral analysis method employs narrow time windows which individually do not contain the entire phase. If any energy at a particular frequency remains outside a given window, then the amplitude at that frequency and group speed will have an apparent geometrical spreading term greater than 0.5.

We have investigated the effect of moving window spectral analysis on geometrical spreading with an experiment using synthetic seismograms.  $L_g$  was synthesized at distances and azimuths corresponding to the stations along the

profile by summing the fundamental and first 25 Rayleigh wave modes for an attenuation-free Great Basin model (Priestley and Brune, 1978). The seismograms were then processed in the manner described above, and the amplitude versus distance data were used to determine apparent geometrical spreading as function of frequency and group speed. The results are plotted in Figure 5 which shows that geometrical spreading is fairly constant for those frequencies and group speeds for which there is signal. Figure 5 also shows the average apparent geometrical spreading at each frequency in the group speed window 3.7 to 3.0 km/sec., corresponding to  $L_g$ . It can be seen that the decay term is, for the most part, greater than 0.5, although there is some scatter.

The above experiment indicates that a geometrical spreading term of 0.6 is more appropriate than 0.5 at most frequencies, although at other frequencies terms in the range 0.4 to 0.6 are obtained. In order to determine how significant the scatter is, we processed the data recorded along the profile assuming geometrical spreading terms of 0.0 to 1.2 in steps of 0.1 and solved for  $Q$ . Average  $Q$  at each frequency was obtained for  $L_g$  windows of 3.7 to 3.0 km/sec and  $P_g$  windows of 6.0 to 4.5 km/sec. The  $\log Q$  versus  $\log f$  data were fit by least squares to give, for each spreading term, the function  $Q(f) = Q_0 f^n$ . Figure 6 summarizes the results. The frequency dependence terms obtained for vertical and transverse  $L_g$  vary little with assumed geometrical spreading, and the  $Q_0$  term becomes stable for spreading terms above 0.6. This suggests that (a) the apparent  $Q$  of both vertical and transverse  $L_g$  is frequency dependent, and (b) the scatter in spreading term about 0.6 evident in Figure 5 should not introduce any serious error.

Figure 6 also shows that  $P_g$  behaves differently than  $L_g$  with respect to assumed geometrical spreading. The frequency dependence term for this phase consistently decreases with increasing spreading while the  $Q_0$  term increases. However, if we assume that the actual  $Q$  of  $P_g$  behaves as  $Q_0 f^n$ , then the linear correlation coefficients shown in Figure 6c indicate that an apparent geometrical spreading of less than 0.7 is required.

Assuming an apparent geometrical spreading term of 0.6, we obtained  $Q$  along the profile. Figure 7 shows the results for each frequency and group speed and averaged over windows corresponding to  $L_g$  and  $P_g$ . The fits to the data over the frequency band  $0.3 \leq f \leq 10.0$  Hz are

$$Q(f) = 296 f^{0.51} \quad (6)$$

$$Q(f) = 202 f^{0.57} \quad (7)$$

and

$$Q(f) = 198 f^{0.45} \quad (8)$$

for vertical component  $L_g$ , transverse component  $L_g$ , and vertical component  $P_g$ , respectively. Vertical  $L_g$  has  $Q$  similar to both vertical  $P_g$  and transverse  $L_g$  for frequencies below about 1.5 Hz. Above that, vertical  $L_g$   $Q$  is consistently

greater than the others, except above 10 Hz, where both vertical and transverse  $L_g$  again have similar  $Q$ . There is a pronounced bump in all the plots at 2 to 3 Hz. Since this feature appears for all the phases considered, we suspect that it might be an artifact due to recording site conditions. Finally, vertical  $L_g$  and vertical  $P_g$  both have  $Q$  independent of frequency for the range 4 to 9 Hz.

### Discussion

Our results are in reasonable agreement with those of Cheng and Mitchell (1981) and Singh and Herrmann (1983). Both (4) and (5) yield values of  $Q$  which are within 25% of that found by Cheng and Mitchell, if we assume their results to reflect the  $Q$  at 5 seconds. Our  $Q_0$  values are within the range given by Singh and Herrmann (1983). The frequency dependence obtained here using the earthquake data is in very good agreement with theirs, if we take into account the uncertainties in the two values. Again, the explosion data yield a  $Q$  function with a greater frequency dependence.

Our findings do not support the conclusions of either Peseckis and Pomeroy (1984) or Nuttli (1986). Peseckis and Pomeroy's  $Q_0$  is greater than ours, and we find no evidence to suggest a frequency dependence as low as  $f^{0.3}$ . Nuttli's result of  $f^{0.6}$  is closer to ours; however, his  $Q_0$  is too low, according to our data. Perhaps these discrepancies are indicative of the larger scatter inherent in time domain measurements of frequency dependent quantities. Since all of the previous studies considered only a few paths, it is likely that the results presented here are more representative of the true apparent  $Q$  in the Great Basin.

The discrepancy between the frequency dependence inferred from the explosion versus the earthquake data, if significant, suggest that energy from the two source types does not sample the crust in an identical manner. Campillo et al (1985) present ray tracing diagrams which show that the crustal sampling by  $L_g$  waves is influenced by source depth. Their results suggest that  $L_g$  energy from surface sources (like explosions) propagates primarily in the shallow layers, while an earthquake at 10 km depth generates energy which uniformly samples the entire crust. If this is the case in the great Basin, then our data indicate that there is greater frequency dependence of  $Q$  in the shallow crust than at depth.

### References Cited

- Butler, R., C. S. McCrerry, L.N. Fraser, and D. A. Walker, 1987. High-frequency seismic attenuation of oceanic P and S waves in the western Pacific, *J. Geophys. Res.*, 92, 1383-1396.
- Campillo, M., J. Plantet, and M. Bouchon, 1985. Frequency- dependent attenuation in the crust beneath central France from  $L_g$  waves: data analysis and

numerical modeling, *Bull. Seism. Soc. Am.*, 75, 1395-1411.

Chavez, D. E. and K. F. Priestley, 1986. Measurement of frequency dependent  $L_g$  attenuation in the Great Basin, *Geophys. Res. Lett.*, 13, 551-554.

Cheng, C., and B. J. Mitchell, 1981. Crustal Q structure in the United States from multi-mode surface waves, *Bull. Seism. Soc. Am.*, 71, 161-181.

Evernden, J.F., C.B. Archambeau, and E. Cranswick, 1986. An evaluation of seismic decoupling and underground nuclear test monitoring using high-frequency seismic data, *Rev. of Geophys.*, 24, 143-215.

Knopoff, L., F. Schwab, and E. Kausel, (1973). Interpretation of  $L_g$ , *Geophys. J. R. astr. Soc.*, 39, 389-404.

Nuttli, O. W., 1973. Seismic wave attenuation and magnitude relations for eastern North America, *J. Geophys. Res.*, 78, 876-885.

Panza, C. F., and G. Calcagnille, (1975).  $L_g$ ,  $L_1$ , and  $R_g$  from Rayleigh modes, *Geophys. J. R. astr. Soc.*, 40, 475-487.

Pesekis, L.L., and P.W. Pomeroy, 1984. Determination of Q using  $L_g$  waves and its implications for nuclear yield estimation, *EOS*, 65, 995.

Priestley, K. F. and J. N. Brune, 1978. Surface waves and structure of the Great Basin of Nevada and western Utah, *J. Geophys. Res.*, 83, 2265-2272.

Singh, S., and R. B. Herrmann, 1983. Regionalization of crustal coda Q in the continental United States, *J. Geophys. Res.*, 88, 527-538.

Fig. 1. Map showing the region sampled by our data. The permanent Lawrence Livermore stations are indicated by large squares, dots show the epicenters of the earthquakes recorded at those stations and considered in this study. Small squares are the temporary sites instrumented to record the December 5, 1985 NTS nuclear explosion.

Fig. 2. Reduced record section for the vertical component data recorded along the profile in Figure 1. The windows used to compute the  $L_g$  spectra are marked on each record. The change in signal character at 490 km is due to the different instrument response there.

Fig. 3. Great Basin  $Q(f)$  functions. The light lines are the results using earthquake data, the heavy line is from the explosion profile.

Fig. 4. Examples of moving window spectra for the closest (top) and furthest (bottom) stations along the nuclear explosion profile in Figure 1. Contours are log ground amplitude in microns.

Fig. 5. Apparent geometrical spreading along the profile determined by inverting synthetic data. Bottom figure is average apparent geometrical spreading for the indicated group speed window. The dashed line is at 0.5, the solid line at 0.61 is the average.

Fig. 6. Effect of geometrical spreading on determination of  $Q(f)$  by applying the moving window spectra technique to the data recorded along the profile. Closed circles denote vertical component  $L_g$ , squares denote transverse component  $L_g$ , and triangles denote vertical component  $P_g$ . Arrows in (a) and (b) indicate the term solved for by fitting average log  $Q$  and log frequency values for group speed windows appropriate for the phases  $L_g$  and  $P_g$ ; (c) is the linear correlation coefficient obtained from the least-squares fits.

Fig. 7. Apparent  $Q$  functions for vertical and transverse  $L_g$  and vertical  $P_g$ , obtained by the moving window spectral analysis technique assuming a geometrical spreading term of 0.6. Error bars represent the standard deviation in apparent  $Q$  at each frequency for averages over 3.7 to 3.0 km/sec for  $L_g$  and 6.0 to 4.5 km/sec for  $P_g$ . Least-squares fit to the data yield the relationships indicated.

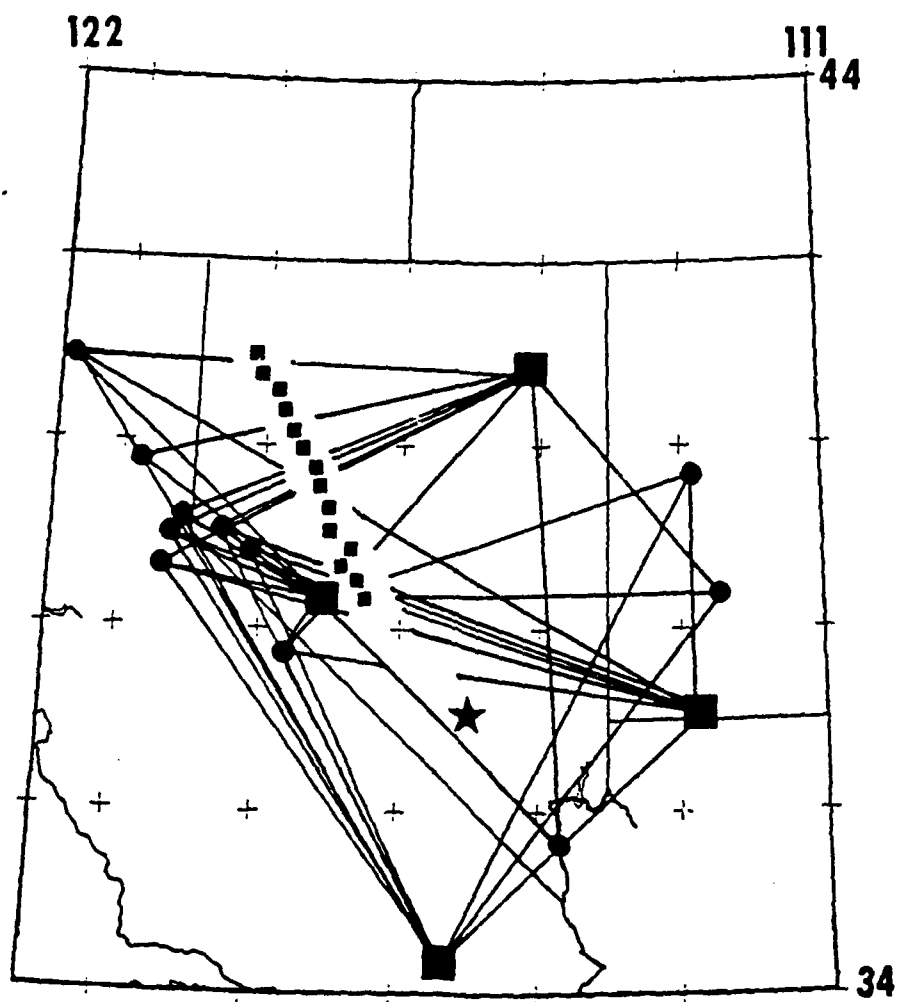


Figure 1

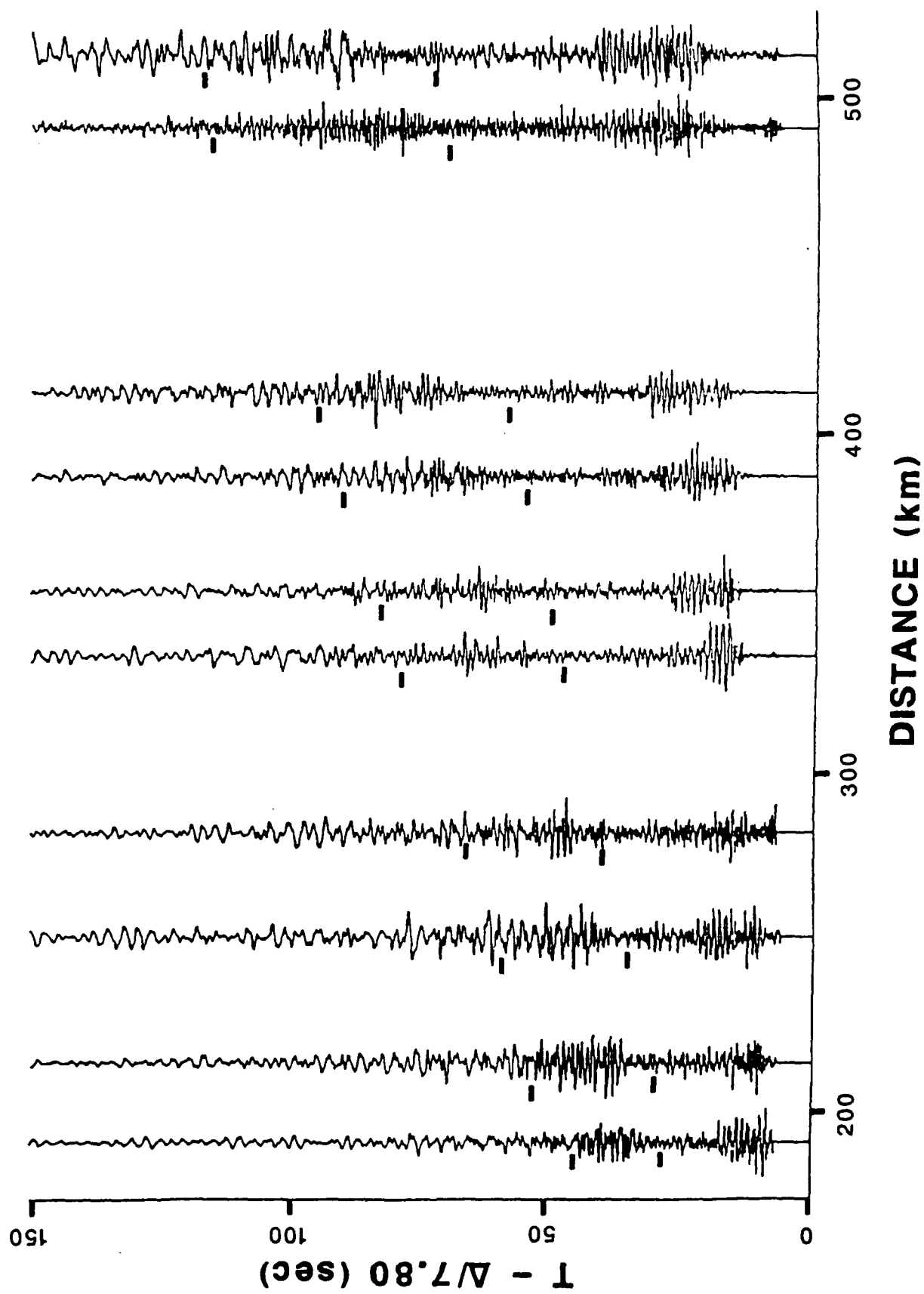


Figure 2

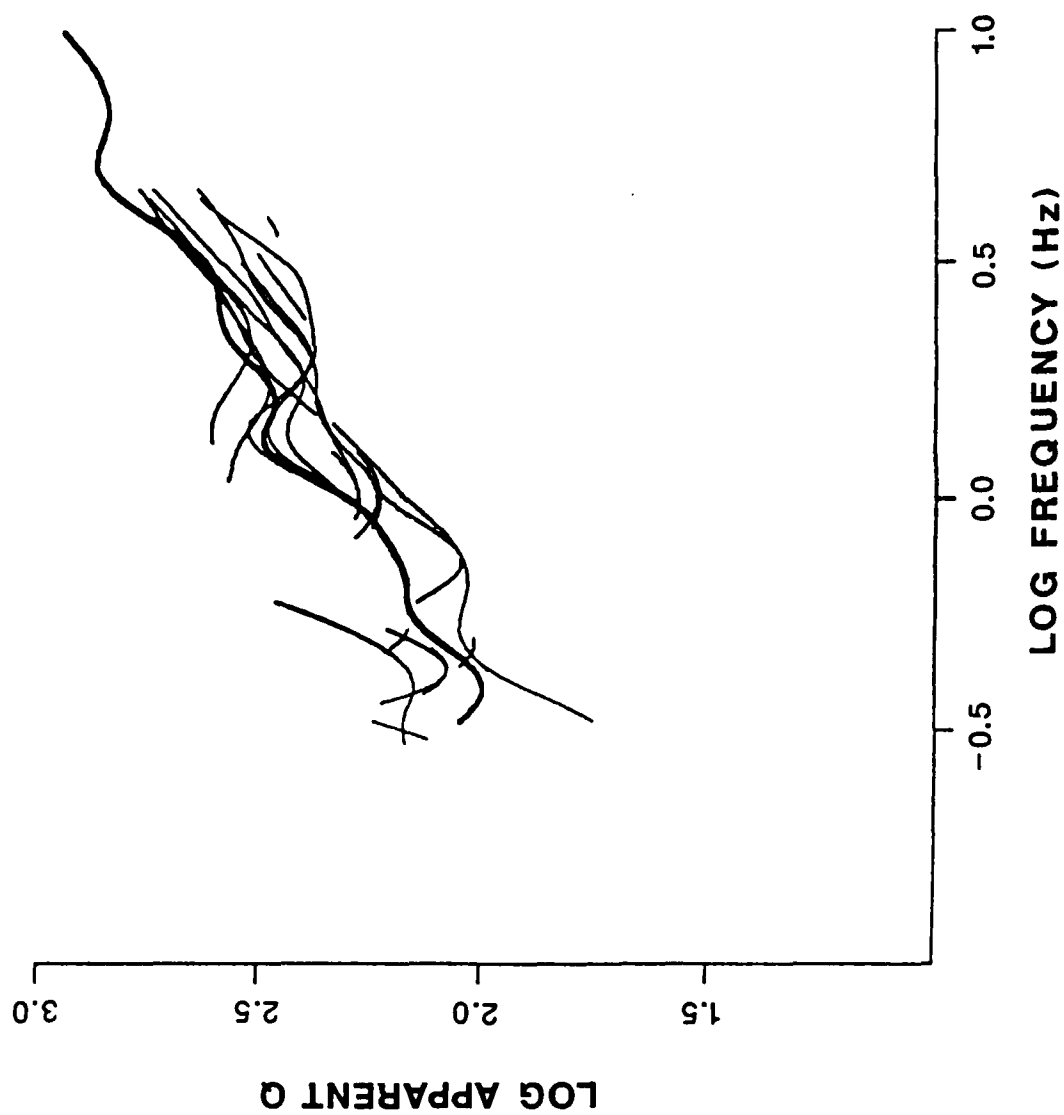


Figure 3



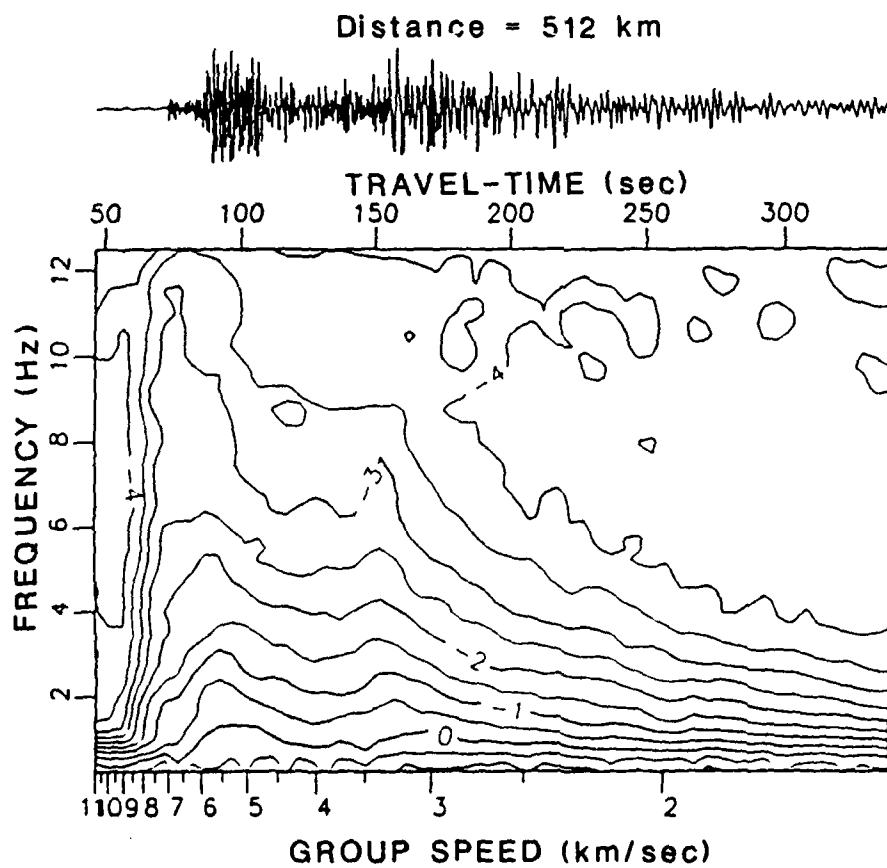
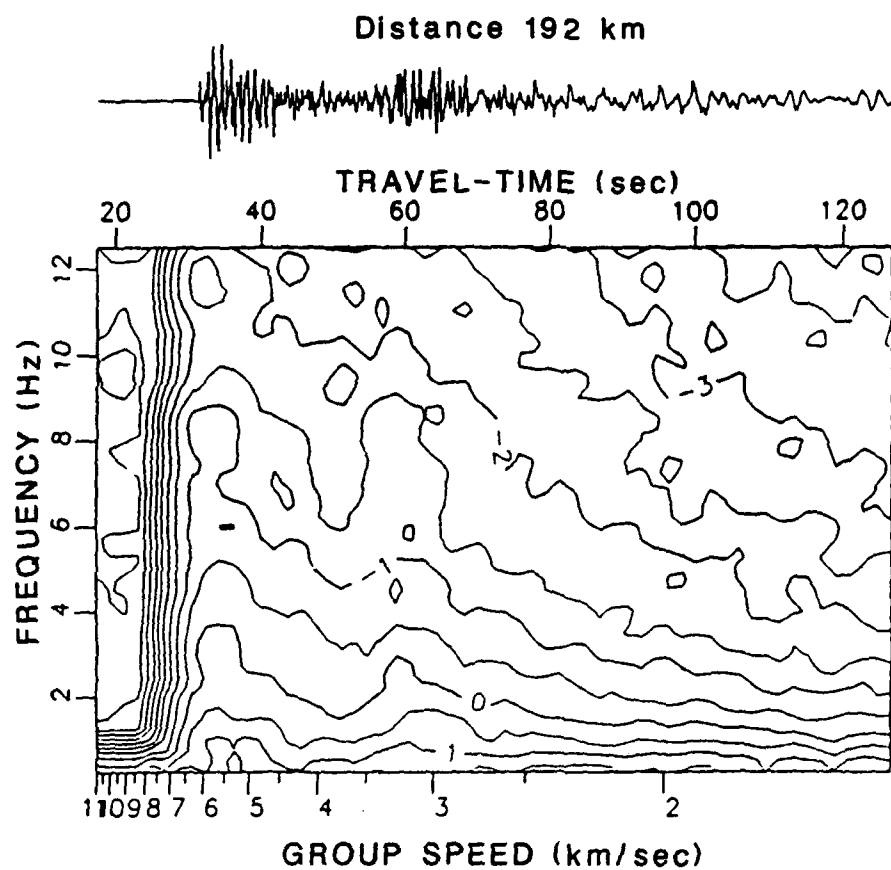


Figure 4

# GEOMETRICAL SPREADING COEFFICIENT

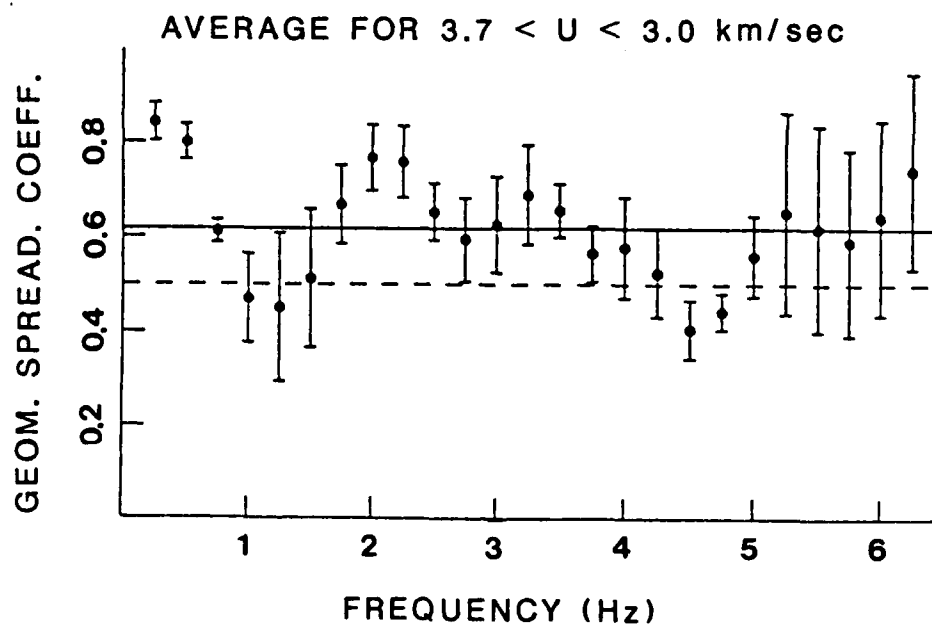
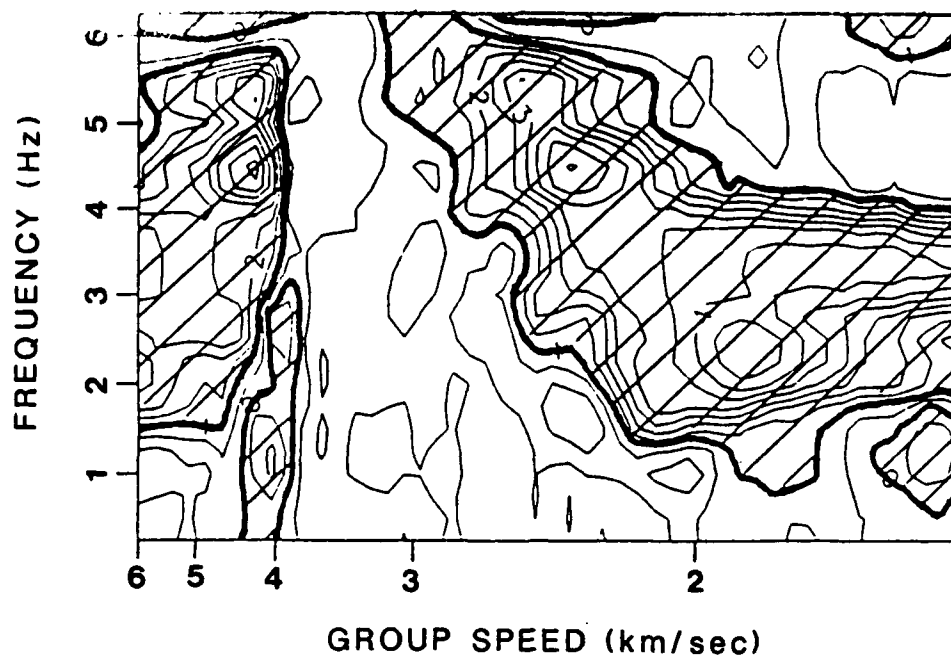


Figure 5

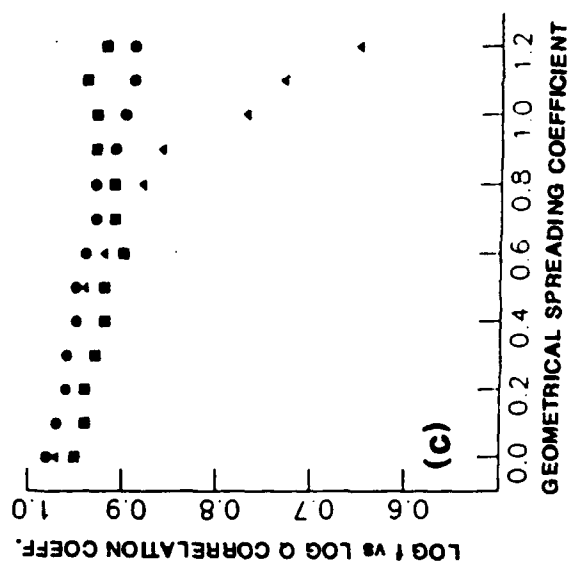
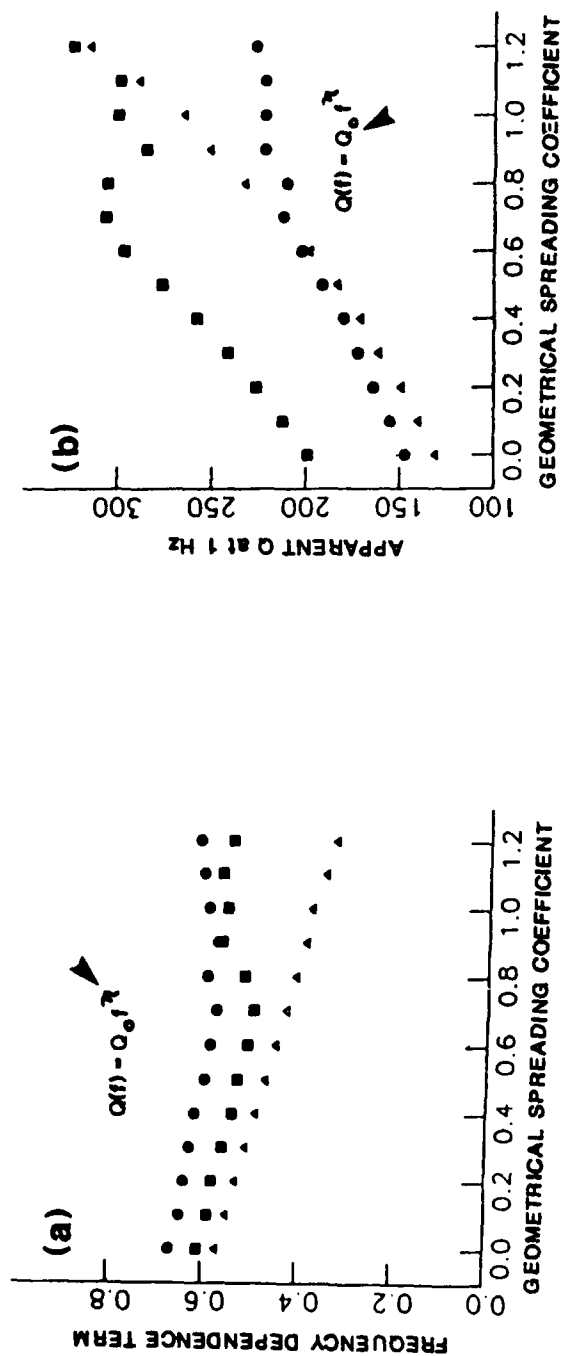


Figure 6

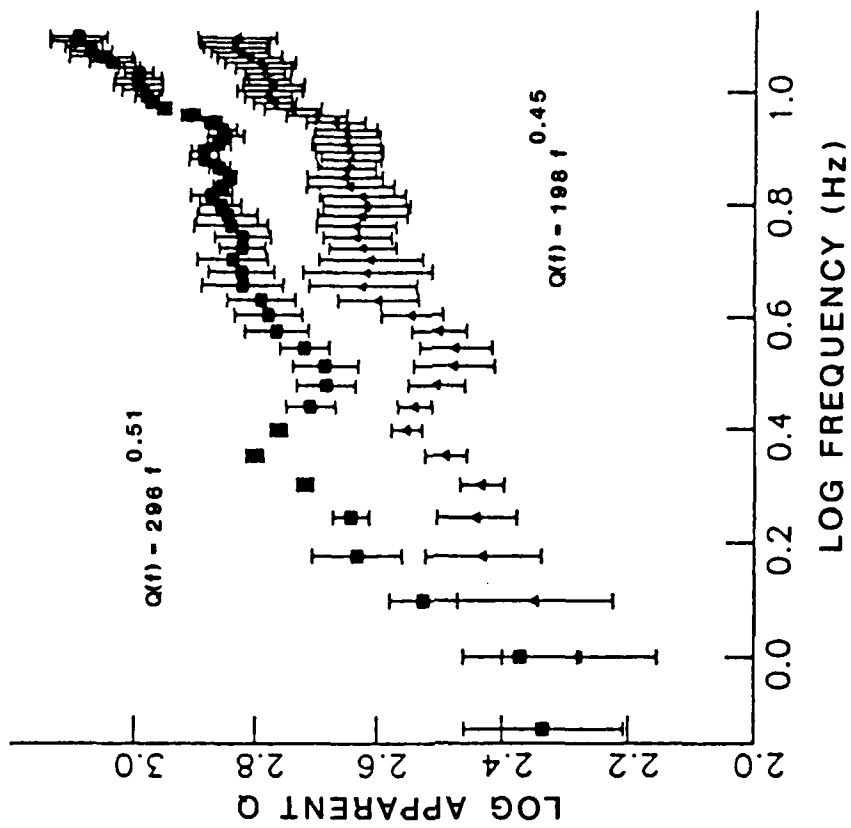
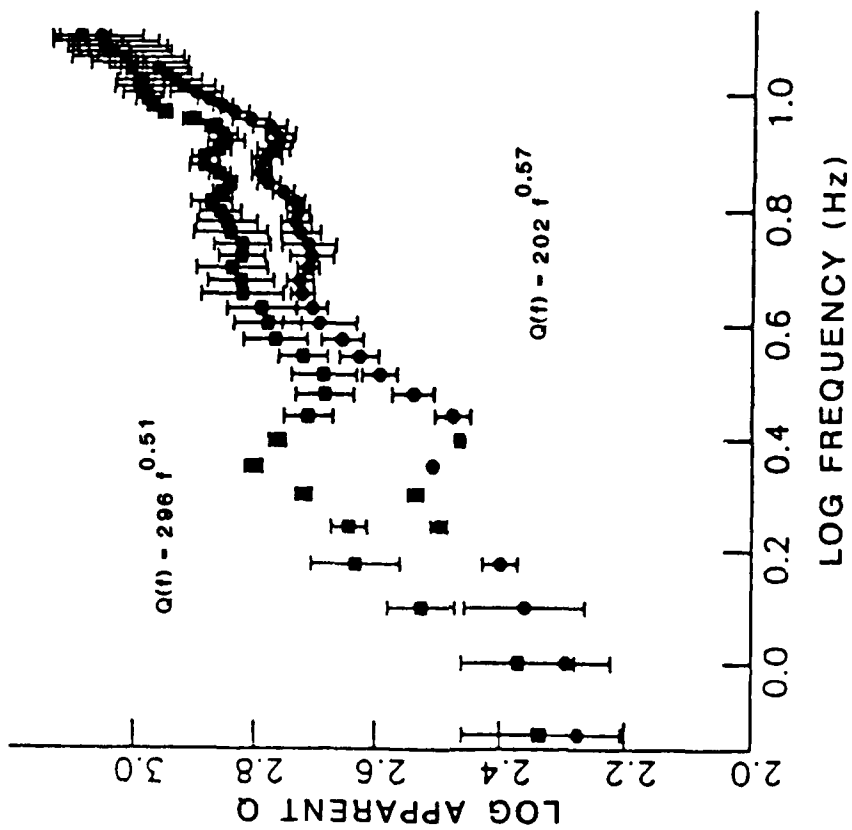


Figure 7

# REGIONAL SEISMIC RECORDINGS OF THE SOVIET NUCLEAR EXPLOSION OF THE JOINT VERIFICATION EXPERIMENT

Keith F. Priestley, William R. Walter

Seismological Laboratory, University of Nevada, Reno

Valadic Martynov, Mikhail V. Rozhkov

Institute of the Physics of the Earth, Soviet Academy of Science, Moscow, U.S.S.R.

**Abstract.** During August and September, 1988, the United States and the Soviet Union conducted a Joint Verification Experiment in which each country was permitted to observe a nuclear explosion at the other country's test site using hydrodynamic means. We have seismically recorded the Soviet explosion at four stations at regional distances ( $\Delta \leq 750$  km), and here report those observations. The peak-to-peak particle motion in the P-wave varied from  $7.54 \times 10^{-1}$  cm/sec at  $\Delta = 160$  km to  $1.02 \times 10^{-2}$  cm/sec at  $\Delta = 740$  km. The average  $m_b(L_g)$  was 5.97 corresponding to a yield of 118 KT, based on the NTS  $m_b(L_g)$  - yield relation of Patton [1988]. The average  $P_n$  corner frequency of the Soviet explosion was 4 Hz with evidence of a second corner at about 0.7 Hz. Both of these corners could be affected by spall. Near-regional seismograms of the Soviet JVE explosion show a large arrival within the  $L_g$  phase on the transverse component at all four sites. This may correspond to tectonic release accompanying the explosion, or to the effects of anisotropy on seismic wave propagation.

## Introduction

During August and September, 1988, the United States and the Soviet Union conducted a Joint Verification Experiment (JVE) for the purpose of calibrating yield measurements at their nuclear weapons testing sites. Scientists from each country were permitted to observe a nuclear explosion at the other country's test site using hydrodynamic means. In addition, as part of the official experiment each country made teleseismic ( $\Delta > 2500$  km) measurements at five national seismograph stations in the U.S. and five in the Soviet Union. The Natural Resources Defense Council (NRDC) reached an agreement with the Soviet Academy of Science (SAS) to make additional seismic recordings of the Soviet JVE explosion in the Soviet Union at regional distance ranges ( $< 2500$  km). Here we present preliminary analysis of the seismic data recorded at four sites in Eastern Kazakhstan at distances less than 750 km.

## Seismic Instrumentation

Seismic data for the Soviet JVE nuclear explosion were recorded at four sites in Eastern Kazakhstan. Three seismo-

graphs were at the previously occupied NRDC-SAS sites [Berger et al, 1987] surrounding the Soviet test site at near-regional distance range: Karasu (KSU,  $\Delta = 160$  km), Karaklinsk (KKL,  $\Delta = 255$  km), and Bayanul (BAY,  $\Delta = 255$  km). The fourth instrument was located at the SAS seismograph site at Talgar (TLG,  $\Delta = 740$  km) to the south of the nuclear weapons testing site. The locations of the recording sites and of the explosion are shown in Figure 1.

The four seismograph sites lie within the Kazakh fold system, a belt of folded and faulted Paleozoic rocks [Leith, 1987]. The region was marked by extensive igneous activity during the late Hercynian Orogeny in the Permian-Triassic Period. KSU, KKL, and BAY are located on similar granitic intrusions of Paleozoic to early Mesozoic rocks. The granites were intruded into deformed Paleozoic sedimentary rocks. Subsequent tectonic activity has resulted in regional crustal uplift and thickening. The SAS seismograph station at TLG is situated on the northern flanks of the Zaili-Alatau mountains and is sited within Precambrian and Lower Paleozoic crystalline rocks. The most prominent structural feature in the area is the Chingiz fault which cuts northwest to southeast across the Soviet test site. There are indications of rejuvenated movement along the fault during the Neogene and Quaternary [Zhuravlev and Uspensky, 1971]. Geological exposures in the vicinity of the Soviet

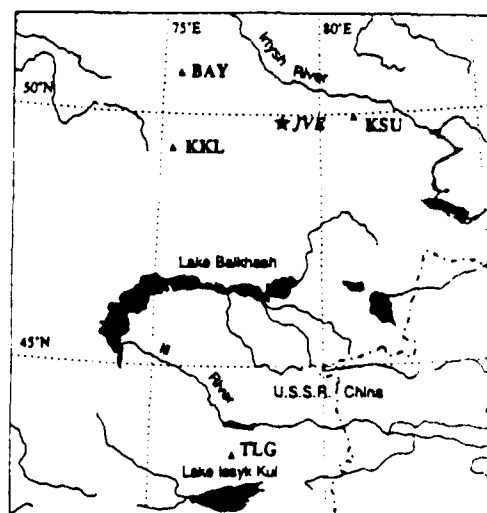


Fig. 1. Location of the four regional seismograph stations KKL, BAY, KSU, and TLG, and the location of the Soviet JVE explosion.

Copyright 1990 by the American Geophysical Union.

Paper number 89GL03095.

0094-8276/90/89GL-03095\$03.00

The U.S. Government is authorized to reproduce and sell this report. Permission for further reproduction by others must be obtained from the copyright owner.

test site suggest the area is fairly heterogeneous. Despite the geological complexity, Ruzashin et al. [1977] find efficient  $L_g$  propagation across the Kazakh fold system.

The characteristics of the three near-regional sites KSU, KKL, and BAY have been described by Berger et al. [1988]. The permanent NRDC-SAS seismographs previously operating at KKL, BAY, and KSU [Berger et al., 1987; 1988] had been removed in late 1987. We reinstalled short- and long-period seismographs in each of the vaults to record the Soviet JVE nuclear explosion. The short-period seismographs consisted of three component Teledyne Geotech S-13 1 second free period seismometers and EDA PRS-4 digital data loggers. The long-period seismographs consisted of a three component Teledyne Geotech SL210/220 15 second free period seismometers and a Kinometrics PDR-2 digital data logger. All these data were sampled at 200 Hz, with the exception of the short-period seismograph at BAY which was sampled at 100 Hz. At TLG the sensors are SM-3, 1.6 sec free period seismometers. Data are recorded at 100 Hz on the PUSK-2, a 120 dB dynamic range digital data logger developed jointly by the Soviet and Georgian Academy of Sciences.

### Data

Examples of the short-period vertical component seismograms for the Soviet JVE explosion are shown in Figure 2. The KKL seismogram shows an emergent, low frequency first arrival, followed about three-quarters of a second later

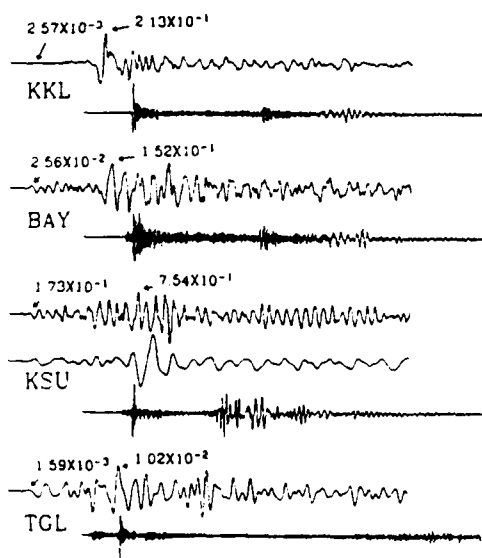


Fig. 2. Short-period vertical seismograms of the Soviet JVE explosion recorded at the four regional seismograph sites. The upper part of each section of the figure shows 10 seconds of the P-wave, the lower portion shows 100 seconds of the whole wave train at KKL, BAY and KSU and 150 seconds at TGL. Two expanded plots of the KSU P-wave are shown, the upper is the original data, and the lower is the same data section after low-pass filtering with a butterworth 4 pole filter with the corner at 1.5 Hz. The peak-to-peak particle motion for initial arrival and for the largest amplitude in the first ten seconds is noted and has units of cm/sec.

by a low amplitude, higher frequency arrival. KKL is past the  $P_n - P_g$  cross-over distance predicted from the eastern Kazakhstan velocity structure [Antonova et al., 1978; and Priestley et al., 1988], and we assume the low frequency first arrival is  $P_n$ . The  $P_g$ -wave train is dominated by the large amplitude dilatational arrival on the vertical and radial components following the first  $P_n$  arrival by about 1.5 sec. The dilatational motion of this arrival suggest a supercritical reflection from the Moho. Synthetic reflectivity seismograms computed for the Priestley et al. [1988] velocity structure agree in both the  $P_n - P_mP$  interval time and in the relative amplitudes observed at KKL, as well as for observations of the same phase at BAY and KSU. There is a well developed  $L_g$  phase seen on the vertical component, but as discussed below, the  $L_g$  amplitudes are largest on the transverse component.

The BAY seismogram shows a more impulsive, larger amplitude and higher frequency  $P_n$  arrival than that observed at KKL. However, like KKL, the BAY P-wave is dominated by a large amplitude dilatational arrival about 1.5 seconds after the initial P-wave arrival (see Figure 4). The vertical component  $L_g$  at BAY is similar to that seen at KKL. The maximum amplitude in the  $L_g$  phase observed at BAY is also on the transverse component. However, most of the  $L_g$  energy in the transverse BAY record occurs in a single pulse.

The closest recording of the Soviet JVE was made at KSU, within the  $P_n - P_g$  crossover distance. Both the short and long-period recordings from KSU show the characteristic 3 Hz resonance associated with the site (upper KSU recording in Figure 2). Neither previous borehole recordings [Berger et al., 1988], nor nearby recordings ( $\approx 200$ m) outside the vault [Myers, personal communication, 1988] show as strong a resonance indicating that it is not characteristic of the site in general, but of the pier in the vault. We have also included a lowpass filtered time series to remove the effect of the site resonance. This filtered seismogram of KSU shows a large amplitude arrival following the first arrival by about 2 seconds, corresponding to the time for the  $P_mP$  reflection at this distance.

The TLG recording was made at a much larger distance than the other recordings. The largest phase on the vertical seismogram has an amplitude of  $4.27 \times 10^{-2}$  cm/sec, with a group velocity of 7.18 km/s. There is a well developed  $L_g$  phase at TLG with the maximum amplitude in the  $L_g$  wave train on the transverse component.

### Preliminary analysis

Figure 3 shows the instrument corrected (solid line), whole-path Q-corrected (dashed line), and noise (dotted line) spectra for the  $P_n$ ,  $P_g$ , and  $L_g$  phases from the long-period vertical component seismogram recorded at BAY. The KKL spectra are almost identical to those computed from the BAY recording. The dashed  $L_g$  spectra is corrected for Q using our unpublished attenuation results ( $Q_{L_g} = 367 f^{0.48}$ ). We have made the often used assumption (e.g. Evernden et al. [1986]) that  $Q_{P_g} / Q_{L_g} = 2.25$ , so  $Q_{P_g} = 825 f^{0.48}$ , in plotting the dashed  $P_g$  spectrum. The dashed  $P_n$  spectrum is corrected for attenuation using the value of  $Q = 9000$  suggested by Evernden et al. [1986].

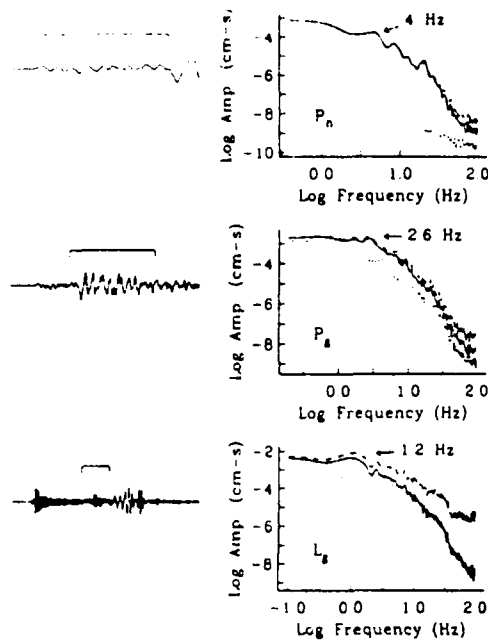


Fig. 3.  $P_n$ ,  $P_g$ , and  $L_g$  spectra for the vertical component seismogram recorded at BAY. The time windows used are indicated above the time series. A 10 percent cosine taper was applied prior to transforming. The corner frequency is noted on the spectra. The solid curve is the spectrum of the indicated phase. The dashed curve is the attenuation corrected spectrum using the values quoted in the text. The dotted curve is the spectrum of the noise. For  $P_n$  and  $P_g$  the noise spectra was computed by transforming an equal length time series immediately before the first P-wave arrival; for  $L_g$  an equal length time series immediately before the  $L_g$  arrival was used.

The  $P_n$  and  $P_g$  spectra shows a good signal to noise ratio to at least 50 Hz. If we parameterize the  $P_n$  and  $P_g$  spectra with a two line model between 1 and 30 Hz, the uncorrected spectra show similar behavior with corner frequencies of about 4 Hz and falloff slopes above the corner approximately proportional to  $\omega^{-3}$ . There is a suggestion of a second corner in the spectra at about 0.7 Hz. The corrected spectra show about the same corner frequency and a slightly shallower high frequency falloff. If the actual attenuation for  $P_g$  is closer to  $Q_{L_g}$ , as some scattering studies suggest, the falloff slope becomes closer to  $\omega^{-2}$ . The  $L_g$  spectrum shows signal above the noise to about 3 Hz.

The average corner frequency for the Soviet explosion is somewhat higher than corner frequencies of similar size nuclear explosions detonated at NTS recorded at comparable distances. The lower corner frequencies of the U.S. explosions may reflect the higher crustal and upper mantle attenuation in the Basin and Range, or possibly a lower coupling coefficient of the weaker rocks in the Nevada Test Site. However, for NTS explosions of about the same size, spall affects frequencies in the range 0.5 to 2.0 Hz [Taylor and Randall, 1988]. We have no knowledge of the spall characteristics of the Soviet test site and cannot eliminate differences in spall between the two testing areas as the cause of the differences in the spectra.

Figure 4 shows the transverse component seismograms after rotating the horizontal components to radial and transverse. These seismograms show significant energy at the  $S_g / L_g$  arrival time. The BAY seismogram shows a remarkably strong coherent SH arrival on the transverse component. This is the largest amplitude arrival on the BAY seismogram. KKL and KSU also show significant SH energy, however this is spread out over several seconds duration. The filtered BAY seismograms show a distinct Love wave arrival on the transverse component preceding the Rayleigh wave on the vertical and radial components. Previous studies have noted anomalous surface wave radiation from Semipalitinsk nuclear explosions [Rygg, 1979]. These observations have been attributed to tectonic release equivalent to motion on thrust faults dipping  $45^\circ$ . However, there have been suggestions that apparent quadrupole seismic radiation from explosions may arise from the anisotropic properties of the source or propagation medium (e.g. Mandal and Toksoz, 1989).

Nutli [1973] defined a magnitude  $m_b(L_g)$  based on the amplitudes of 1 second  $L_g$  waves, and Nutli [1986a] argued for the usefulness of  $m_b(L_g)$  in estimating yields of NTS nuclear explosions. Nutli [1986b, 1987] used  $L_g$  arrivals from Soviet nuclear explosions in eastern Kazakhstan which were recorded in western Europe and southern Asia to estimate yields of Soviet explosions. The greatest uncertainty in the  $m_b$  - yield relationship arises from uncertainties in the attenuation function used for correcting the  $L_g$  amplitudes for the effects of anelasticity. Since we have made direct measurements of the  $L_g$  attenuation only in the region of the

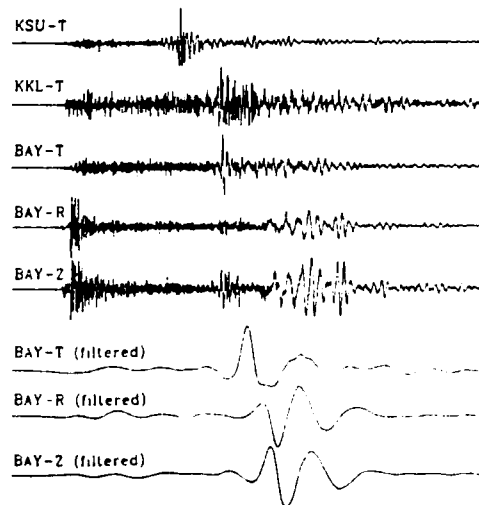


Fig. 4. Transverse component recordings of the Soviet JVE at KSU, KKL and BAY are shown at the top of the figure. The KSU trace is the short-period record low pass filtered at 1.5 Hz. The remaining traces are long-period broadband seismograms. Also shown for comparison are the radial and vertical components at BAY. At the bottom of the figure low-pass filtered (corner of 0.2 Hz) transverse, radial and vertical BAY seismograms are shown. Each trace is self-scaled. The filtered BAY seismograms show significant Love waves. The absolute amplitude of the filtered BAY transverse component is about four times smaller than the vertical component.

Soviet test site, we have used only  $L_g$  recordings from BAY, KKL and KSU in estimating  $m_b(L_g)$ . The  $m_b(L_g)$  for the Soviet JVE is  $5.689 \pm 0.002$ . Nuttli (1986a, 1986b, 1987) argues for the portability of  $m_b$  - yield relationships derived from NTS data; however, Patton [1988] cautions that coupling differences may have a significant influence. An  $m_b(L_g)$  of 5.689 corresponds to a yield of 148 KT using the Nuttli [1986]  $m_b(L_g)$  - yield relation and 118 KT using the Patton [1988]  $m_b(L_g)$  vs. yield relation, both of which are based on NTS data. Sykes and Ekstrom [1989] using a combined  $m_b$  and  $M_s$  magnitude - yield relation have estimated the yield of the Soviet JVE to be 113 KT.

### Summary

Broadband regional seismograms of the 1988 Soviet JVE at four sites in the U.S.S.R. have been shown. The P wave spectra show good signal-above-noise up to at least 50 Hz. The transverse components show significant energy at the  $S_g / L_g$  arrival time, and Love waves at longer periods. This Soviet JVE data provides an opportunity to test methods of analysis, developed in other areas, on data recorded wholly within the U.S.S.R. Using one such method, the  $m_b(L_g)$  - yield relations developed for NTS, we have estimated the yield of this event.

**Acknowledgements.** We thank Steve Taylor, George Zandt, and George Randell for helpful discussions. Christina Hackman of the University of Colorado and Kenneth Smith of the University of Nevada helped in the data collection effort. The data collection was supported by a grant from the Natural Resources Defense Council. This research was partially supported by grants from the Air Force Geophysical Laboratory under contract number F19628-87-K-009, the Lawrence Livermore National Laboratory under contract number W-7405-ENG-48, and the National Science Foundation under contract number EAR8708506.

### References

- Antonova, L. V., F. F. Aptikayev, R. I. Kurochkina, I. L. Nersesov, A. V. Nikolayev, A. I. Ruzaykin, Y. N. Sedova, A. V. Sitnikov, F. S. Tregub, L. D. Fedorskaya, and V. I. Khaturin, *Experimental Seismic Investigation of the Earth's Interior*, AS USSR, Institute of Physics of the Earth, Publishing House "Nauka", Moscow, 155p, 1978.
- Berger, J., J. N. Brune, P. A. Bodin, J. S. Gombert, D. M. Carrel, K. F. Priestley, D. E. Chavez, W. R. Walter, C. B. Archambeau, T. B. Cochran, L. L. Nersesov, M. B. Gokhberg, O. A. Stolyrov, S. K. Daragen, N. D. Tarasov, Y. A. Sutelov, A new US - USSR seismological program, *EOS*, 68, 105, 110-111, 1987.
- Berger, J., H. K. Eissler, F. L. Vernon, I. L. Nersesov, M. B. Gokhberg, O. A. Stolyrov, and N. T. Tarasov, Studies of high-frequency seismic noise in Eastern Kazakhstan, *Bull. Seismol. Soc. Am.*, 78, 1744-1758, 1988.
- Evernden, J., C. Archambeau, and E. Cranswick, An evaluation of seismic decoupling and underground nuclear test monitoring using high frequency seismic data, *Rev. Geophys.*, 24, 143-215, 1986.
- Leith, W., Geology of NRDC seismic stations in Eastern Kazakhstan, USSR, *USGS Open-File Report* 87-597, 1987.
- Mandal, B., and M. Toksoz, Radiation patterns from explosions in anisotropic media, paper presented at DOE/LLNL symposium on explosion-source phenomenology, March 14-16, 1989, Lake Tahoe California.
- Nuttli, O., Seismic wave attenuation and magnitude relations for eastern North America, *J. Geophys. Res.*, 78, 876-888, 1973.
- Nuttli, O., Yield estimates of Nevada Test Site explosions obtained from seismic  $L_g$  waves, *J. Geophys. Res.*, 91, 2737-2151, 1986a.
- Nuttli, O.,  $L_g$  magnitudes of selected East Kazakhstan underground explosions, *Bull. Seism. Soc. Am.*, 76, 1241-1251, 1986b.
- Nuttli, O.,  $L_g$  magnitudes at Deglen, East Kazakhstan underground explosions, *Bull. Seism. Soc. Am.*, 77, 679-681, 1987.
- Patton, H. J., Application of Nuttli's method to estimate yield of Nevada Test Site explosions recorded on Lawrence Livermore National Laboratory's digital seismic system, *Bull. Seism. Soc. Am.*, 78, 1759-1772, 1988.
- Priestley, K. F., G. Zandt, and G. E. Randall, Crustal structure in Eastern Kazakh, U.S.S.R. from teleseismic receiver functions, *Geophys. Res. Lett.*, 15, 613-616, 1988.
- Rygg, E., Anomalous surface waves from underground explosions, *Bull. Seism. Soc. Am.*, 69, 1995-2002, 1979.
- Ruzkin, A. I., I. L. Nersesov, V. I. Khaturin, and P. Molnar, Propagation of  $L_g$  and lateral variations in crustal structure in Asia, *J. Geophys. Res.*, 82, 307-376, 1977.
- Sykes, L., and G. Ekstrom, Comparison of seismic and hydrodynamic yield determinations for the Soviet joint verification experiment of 1988, *Proc. Natl. Acad. Sci. USA*, 86, 3456-3460, 1989.
- Taylor, S. R., and G. E. Randall, The effects of spall on regional seismograms, *Geophys. Res. Lett.*, 16, 211-214, 1989.
- Zhuralev, B. Y., and E. P. Uspensky, Large faults of the Chingiz range, American Geophysical Union translation, *Geotectonics*, 5, 305-309, 1971.
- K. Priestley and W. Walter, Seismological Laboratory, University of Nevada, Reno, Reno, NV 89557.
- V. Martynov and M. Rozhkov, Institute of the Physics of the Earth, Soviet Academy of Science, Moscow, U.S.S.R.

(Received: August 25, 1989;

Accepted: September 27, 1989)



# Observations of High-Frequency *P* Wave Earthquake and Explosion Spectra Compared With $\omega^{-3}$ , $\omega^{-2}$ , and Sharpe Source Models

WILLIAM R. WALTER, JAMES N. BRUNE, AND KEITH F. PRIESTLEY

*Seismological Laboratory, Mackay School of Mines, University of Nevada at Reno*

JON FLETCHER

*U.S. Geological Survey, Menlo Park, California*

Observations of 10-, 20-, and 30-Hz *P* wave spectral amplitudes from earthquakes and explosions are compared with the Archambeau [1968, 1972] earthquake model featuring a *P* wave falloff of  $\omega^{-3}$  beyond the corner frequency, a modified Brune [1970, 1971] earthquake model with  $\omega^{-2}$  falloff, and the Sharpe [1942] explosion model which has a  $\omega^{-2}$  falloff. The Archambeau and Sharpe models have been, in part, the basis of a proposal by Evernden *et al.* [1986] that high-frequency ( $\approx 30$  Hz) seismic energy could provide an effective solution to the problem of detection and identification of low-yield coupled and fully decoupled underground nuclear explosions. The observations of earthquakes show an increase in spectral amplitude with moment approximately in agreement with the  $\omega^{-2}$  falloff model and, for larger moments, in disagreement with the  $\omega^{-3}$  model. Comparison of theoretical and actual seismograms narrow-band filtered at 30 Hz shows that in part the increase in spectral amplitude of earthquakes is due to the complex and long duration of the rupture process and not because of an increase in an impulsive first arrival like that characteristic of an explosion. The 30-Hz amplitudes for explosions show much scatter, and many events have a spectral falloff greater than the  $\omega^{-2}$  predicted by the Sharpe model. Whether this is due entirely to attenuation or is the actual source spectrum is not determined. High stress drop earthquakes are predicted to have larger spectral amplitudes than the Sharpe model. Thus any discrimination technique using high-frequency *P* wave spectra should probably take into account differences in pulse shape and amplitude in the time domain.

## INTRODUCTION

This paper compares observations of *P* wave spectral amplitudes at 10, 20, and 30 Hz from numerous earthquakes and explosions, covering a range of magnitudes, with several theoretical predictions. In particular the spectral amplitudes are compared with the Sharpe [1942] explosion model and with the Archambeau [1968, 1972] earthquake stress relaxation model. The difference in spectral amplitudes between these two models is the basis of a method for discriminating between earthquakes and underground nuclear explosions suggested by Evernden *et al.* [1986]. A preliminary report on the results of these studies was given by Brune *et al.* [1986a].

Evernden *et al.* [1986] proposed that an effective solution to the problem of detection and identification of low-yield coupled and fully decoupled underground explosions was available using high-frequency seismic data ranging up to 30 or 40 Hz. The proposal is based on the theoretical predictions of radiated *P* wave seismic spectra corresponding to the Archambeau [1968, 1972] model for earthquake sources and the Sharpe [1942] model for explosion sources. The Archambeau [1968, 1972] theoretical model for an expanding stress-relaxation (failure) zone has been refined and developed by Minster [1973], Stevens [1980], and Archambeau and Minster [1978] among others. Various models used nonspherically expanding or translating spherical failure zones to simulate time-dependent ellipsoidal failure zones. Stevens [1980] showed that the volume relaxation source formulation used in earlier work could be expressed in terms of failure boundary surface integrals (stress pulse equivalents). Thus in the limit it seems that

these volume stress-relaxation models could be modified to give the same results as the more physically reasonable models involving stress relaxation on a plane, e.g., as in finite element modeling of Archuleta and Frazier [1978], or idealized approximate stress pulse models such as that of Brune [1970, 1971]. However, when one takes into account the inherent complexities in the actual rupture process, it is unlikely that any of these idealized models adequately represents the spectra of most earthquakes. Much evidence indicates that earthquake ruptures are complex multiple events [Wyss and Brune, 1967; Trifunac and Brune, 1970; Kanamori and Stewart, 1978]. Recognition of this fact has stimulated numerous theoretical and numerical models involving complexity [Haskell, 1964; Aki, 1972; Brune, 1970; Blandford, 1975; Papageorgiou and Aki, 1983a, b; Kanamori 1979; Munguia and Brune, 1984]. Recent high quality data from the Anza seismic array [Berger *et al.*, 1984; Fletcher *et al.*, 1987] have indicated that this complexity extends down to small events [Brune *et al.* 1986b; Frankel *et al.*, 1986].

The theoretical *P* wave explosion spectra used by Evernden *et al.* [1986] is that proposed by Sharpe [1942] and independently developed by Latter [1961]. In the Sharpe theory the explosion is modeled as an arbitrary pressure function applied to the interior of a spherical surface at an "elastic radius" from the source. The elastic radius is defined as the distance from the detonation point to the surface beyond which the medium responds linearly (elastically) and thus is a purely medium-dependent property for a given maximum pressure amplitude. For a perfectly decoupled or over-decoupled explosion in a cavity, the elastic radius is the cavity radius. For a tamped or underdecoupled explosion, the elastic radius is larger than the perfectly decoupled cavity radius for the same yield explosion, since the coupling factor in a solid medium is larger than the coupling factor in air. The Sharpe model as used by Evernden *et al.* [1986] (and as developed by Latter [1961]) has a step or Heaviside function in pressure acting at the elastic ra-

Copyright 1988 by the American Geophysical Union.

Paper number 7B5069.  
0148-0227/88/007B-5069\$05.00

The U.S. Government is authorized to reproduce and sell this report. Permission for further reproduction by others must be obtained from the copyright owner.

dius. Other elastic radius models such as that of *Mueller and Murphy* [1971] use a pressure function with an initial spike which decays exponentially to a constant value. This model has more high-frequency energy at and above the corner frequency than the pressure step function Sharpe model. *Evernden et al.* [1986] argue based on the Mueller-Murphy model and finite difference calculations by *Patterson* [1966] that the pressure step function Sharpe model is a conservative estimate of the high-frequency *P* wave energy radiated by both tamped and decoupled explosions. We will confine our analysis in this paper to tamped explosions.

One of the factors of crucial importance in the *Evernden et al.* proposal is the shape of the *P* wave spectrum beyond the corner frequency. The *Archambeau* [1968, 1972] model for earthquakes (with the rupture velocity approximately equal to the shear wave velocity) predicts a high-frequency falloff, beyond the corner frequency proportional to  $\omega^{-3}$ . For simplicity in this paper we will refer to the model as the W3P model ( $\omega^{-3}$  falloff for *P* waves). This kind of falloff has the paradoxical result that for a given stress drop, very large earthquakes do not radiate any more high frequency energy than small earthquakes ( $m_b \approx 1.8$ ). This is a consequence of the fact that the low frequency spectral level is proportional to the cube of the source dimension, which is exactly cancelled out by the  $\omega^{-3}$  falloff from the corner frequency (which scales inversely with the source dimension). *Evernden et al.* [1986] propose that the  $\omega^{-3}$  falloff of the *P* wave spectrum for the *Archambeau* [1968, 1972] model for earthquakes, being different from the  $\omega^{-2}$  falloff of the Sharpe model, enhances the discrimination achievable from the differences in *P* wave corner frequencies between compatible earthquakes and explosions (compatible in that they have the same low-frequency *P* wave amplitudes).

It should be noted that the W3P model as used by *Evernden et al.* does not take into account phase complexity of earthquakes per se, since only the spectrum is used and not the actual time domain signal (or phase). Thus a conclusion regarding the amplitude spectra of the W3P model for earthquakes does not necessarily argue one way or the other as to whether time domain measurements might be used to distinguish between earthquakes and explosions, since earthquakes are complex long-duration ruptures, whereas explosions are impulsive stress pulses on the inside of some actual or equivalent cavity. (The interrelations between spectra, peak amplitude, complexity, and duration of the signal, and the high frequency falloff have been discussed by *Hanks* [1979].)

The problem of determining the slope of the spectral falloff at high frequencies is greatly complicated by attenuation, scattering, and site effects. The determination of seismic moment, being based on much lower frequencies, is relatively insensitive to these effects. Thus if data from one source region with a constant set of stations and ray paths are compared, any increase in high-frequency spectral amplitude with moment can be attributed to the source. Therefore this paper will address the variation of 10-, 20-, and 30-Hz earthquake and explosion *P* wave spectral amplitudes with seismic moment at 10-km hypocentral distances without making any correction for *Q*.

#### THEORETICAL CURVES

In the *Evernden et al.* [1986] paper, Figure 14 shows the theoretical *P* wave spectra of the W3P model. The theoretical spectra have a constant amplitude up to the corner frequency  $f_c^P$ , given by [*Minster*, 1973]

$$f_c^P = \frac{1}{2\pi L} (3\alpha^2 v_r)^{1/3} \quad (1)$$

and then falls off as  $\omega^{-3}$ . Here *L* is the maximum rupture dimension,  $v_r$  is the rupture velocity, and  $\alpha$  is the *P* wave velocity. The relation between the moment and the low-frequency asymptote for the W3P model was derived from the low-frequency (point source) approximation for a double couple dislocation [*Keilis-Borok*, 1959]

$$M_0 = \frac{4\pi\rho\beta^3 R \Omega_0^S}{R_{\theta\phi}} = \frac{4\pi\rho\alpha^3 R \Omega_0^P}{R_{\theta\phi}} \quad (2)$$

and the moment expression for the W3P model (assuming a Poisson solid) given by [*Minster*, 1973; *Minster and Suteau*, 1977]

$$M_0 = \frac{60\pi}{23} L^3 \sigma \quad (3)$$

In (2)  $\rho$  is the medium density, *R* is the hypocentral distance,  $R_{\theta\phi}$  is the radiation pattern,  $M_0$  is the seismic moment,  $\beta$  is the *S* wave velocity, and  $\Omega_0^S$  and  $\Omega_0^P$  are the *S* and *P* wave zero frequency spectral amplitudes. In (3)  $\sigma$  is the stress drop (or the prestress level). Equating (2) and (3) and solving for  $\Omega_0^P$  gives

$$\Omega_0^P = \frac{5\sigma L^3 R_{\theta\phi}}{23\mu\alpha R} \quad (4)$$

where  $\mu$  is the rigidity. This result was checked with Figure 22 from *Evernden et al.* [1986], which shows earthquake spectra predicted by the W3P model and explosion spectra predicted by the Sharpe model. The vertical axis in their Figure 22 gives relative amplitude on the left-hand scale and  $m_b$  on the right-hand scale. To relate  $m_b$  with moment and low-frequency spectral amplitude we have used the  $m_b$  versus the  $\Omega_0$  spectral level relationship of K. F. Priestley and J. N. Brune (Spectral scaling for the Mammoth Lakes, California, earthquakes, submitted to the *Geophysical Journal of the Royal Astronomical Society*; hereafter referred to as PB88). The values obtained agreed with those predicted by (4) within the uncertainty of determining  $m_b$ . This was further checked with the graph of  $m_b$  versus  $M_0$  given by *Tucker and Brune* [1977] for San Fernando aftershocks, with almost identical results.

The values used for the W3P model are  $\alpha = 6.0$  km/s,  $\rho = 2.8$  g/cm<sup>3</sup>,  $\mu = 3.36 \times 10^{11}$  dyn/cm<sup>2</sup>, and a Poisson medium is assumed. We have further assumed that the rupture velocity is equal to the shear wave velocity. As (1) indicates, decreasing the rupture velocity causes the corner frequency to decrease. *Evernden et al.* [1986] show in their Figure 16 that as the rupture velocity decreases below the shear wave velocity, the spectrum develops an intermediate falloff between the constant low-frequency value and the  $\omega^{-3}$  falloff at frequencies much higher than the corner frequency. Thus the case of the rupture velocity equal to the shear wave velocity gives the maximum spectral amplitudes for *P* waves at all frequencies predicted by the W3P model for a given stress drop and moment. (For rupture rates greater than the shear wave velocity, the *Archambeau* [1968, 1972] model predicts a falloff proportional to  $\omega^{-2}$  beyond the corner frequency.)

For the  $\omega^{-2}$  model of earthquake spectra, we used the *Brune* [1970, 1971] model of source spectra with the added assumption that the *P* wave to *S* wave amplitude ratio at low frequencies is  $(\alpha/\beta)^3$ . The ratio is appropriate for the low-frequency (point source) approximation for a double couple dislocation given in (2). We have also assumed a corner frequency shift for *P* waves relative to *S* waves of  $\alpha/\beta$ , as indicated in several studies [e.g.,

W2P model. The values used for the medium are the same as the W3P model. Hereafter for simplicity this model will be referred to as the W2P model ( $\omega^{-2}$  falloff for  $P$  waves).

The Sharpe model curves represent both tamped and decoupled explosions. The moment used for the Sharpe curves was derived from the low-frequency-moment relation of (2), as if the source were an earthquake, using the same parameters for the recording medium as the W3P model. In this paper we have used a maximum pressure of elastic response of 130 bars as assumed by *Fecoluden et al.* [1986] in estimating the spectral amplitude from explosions at the Nevada test site. We have also assumed shot medium parameters of  $\alpha = 3.5$  km/s and  $\rho = 2.0$  g/cm<sup>3</sup>. All the theoretical curves presented in this paper have been normalized to 10-km hypocentral distance and multiplied by a factor of 2 to approximate the free surface effect.

### DATA

There are numerous sources of good high-frequency data now available as a result of the advent of high dynamic range digital event recorders [e.g., *Brune et al.*, 1980] and telemetered arrays [Berger et al., 1984; Fletcher et al., 1987]. The earthquake data used in this study are recordings from the permanent Anza array in southern California [Berger et al., 1984; Fletcher et al., 1987], and temporary digital instruments deployed to record aftershocks of the 1978 Oaxaca, Mexico, earthquake [Munguia et al., 1978] and aftershocks of the 1980 Mammoth Lakes earthquakes [Archuleta et al., 1982; Priestley et al., 1985; PB88]. In order to compare the data with the source models with as little distortion due to attenuation and site effects as possible we have used data recorded on solid rock with hypocentral distances as short as possible. All the data have been normalized to a 10-km hypocentral distance and have not been corrected for  $Q$ .

The data presented here are all far-field data in the frequency domain, except for the 1985 Michoacan main shock. The instruments used in this study have a flat response in velocity or acceleration between 5 and 35 Hz. The spectra were determined from vertical component recordings. The data time series range from 3/4 s to several seconds after the initial  $P$  arrival and ending before the  $S$  wave (except for the Michoacan event). The time series were tapered with a 10% cosine taper at each end. A fast Fourier transform was applied to the tapered time series; the magnitude of the result was then rotated (dividing by  $\omega$  for velocity and  $\omega^2$  for acceleration) to displacement. The Anza spectra were then smoothed, and the spectral amplitude determined directly. For the rest of the data, the magnitude of the spectral amplitude at a particular frequency was determined by averaging about a 6-Hz window centered on the frequency of interest (i.e., 27-33 Hz for 30 Hz) using unsmoothed spectra. Where more than one station recording was available for each event, we followed Archuleta et al. [1982] by taking the average of the log of the spectral amplitudes, rather than a simple arithmetic average.

The Anza array is a 10-station, three-component, 16-bit digitally telemetered array, deployed along the San Jacinto fault zone in southern California. We have analyzed events with seismic moments ranging from  $10^{17}$  to about  $10^{21}$  dyn cm and with hypocentral distances from 5 to 20 km. The Anza array sites are on solid rock, and we expect little distortion due to attenuation at these distances. Hough et al. (S. E. Hough, J. G. Anderson, J. Brune, E. Vernon, J. Berger, J. Fletcher, L. Harr, T. Hanks and L. Baker, Attenuation near Anza, California, submitted to *Bulletin of the Seismological Society of America*) and S. E. Hough and J. G. Anderson (Observations of high frequency spectra at Anza, Cali-

fornia: Implications for  $Q$  structure, submitted to *Bulletin of the Seismological Society of America*) have found high  $Q$  values for Anza sites. Recent comparison of spectra recorded in a 30-m-deep borehole and at the surface by Harr et al. [1987] show amplifications up to a factor of 5 in the 10- to 30-Hz range (beyond the expected factor of 2 at a free surface) and significant attenuation of frequencies above 40 Hz. However, this is expected to affect all events in a similar manner and should not change comparisons of events recorded at the same stations. We also have strong motion data for two earthquakes, an  $M \approx 5.0$  and an  $M \approx 4.7$ , that occurred prior to the installation of the Anza array.

The Oaxaca aftershock data were recorded on an eight-station digital array set up after the main shock of November 29, 1978 [Reyes et al., 1978]. These sites were also located on solid rock to minimize attenuation and site effects. These events are generally deeper than events at Anza since they are associated with the subduction zone. They range in hypocentral distances from 10 to 40 km.

The Mammoth events were recorded on digital seismographs deployed during the Mammoth Lakes earthquake sequence in 1980 [Archuleta et al., 1982]. To minimize attenuation we used events recorded at the three stations CON, FIS, and MGE located on rock. The hypocentral distances of these events range from 5 to 20 km.

We have used one very large event, the Michoacan, Mexico, earthquake of September 19, 1985. A network of strong motion accelerographs located on hard rock sites, was installed in the region prior to the event [Anderson et al., 1986]. Three of the accelerographs were directly over the aftershock zone and inferred rupture. We have used the spectra of the entire vertical component of these stations. As a first-order approximation to normalize to

TABLE 1. Parameters for Pahute Mesa, Nevada, Test Site Explosions used in This Study

Event Name	Depth m	Yield* kt	$m_b$	Hypocentral distance km	Station
Alejandro	1064	566	6.1	3.2	L-04
				3.2	L-04
				3.4	Echo Peak
				5.1	L-05
				6.1	L-02
				10.0	L-06
				12.6	L-01
Halfback	819	300	6.1	2.1	S-5
				2.1	S-7
Inlet	819	290	6.0	1.6	S-1
				3.3	S-1
Scotch	977	150	5.7	6.1	S-03
Boxcar	1166	1200	6.3	10.4	S-034
				22.5	S-034
Fann	689	75	5.5	4.2	4
				4.7	6
				6.4	5
				9.7	2
				21.1	W-9
Colwick	633	75	5.5	21.2	W-17
				18.3	W-17
				23.4	W-18
				20.7	W-2
Pepato	680	75	5.5	22.5	W-17
				25.4	W-9
Sheepshead	640	100	5.6	15.1	W-17
				17.7	W-17
				22.8	W-17

\* Yields from Springer and Kinnman [1971], Barker et al. [1982], or estimated from  $m_b$ .

10-km hypocentral distance, we have assumed the energy radiated per unit area is constant at the fault surface, and that energy is conserved. Therefore we multiply the spectral amplitude by the square root of the ratio: twice the fault surface area divided by the area of a sphere at 10 km. This correction increases the spectral amplitude by about a factor of 3.7.

The explosion data used here are underground nuclear explosions from Pahute Mesa on the Nevada test site (NTS). We have several explosions ranging in size from approximately 100 to 1200 kilotons (kt), recorded on velocity and acceleration sensors. The event names, approximate yields, and hypocentral distances are given in Table 1. The hypocentral distances range from 3 to 25 km. The moment for each explosion was determined using the formula

$$M_0 = 18.135 + m_b \quad (5)$$

taken from Priestley and Brune (PB88) (assuming the  $\Omega_0 - M_0$  relation of (2) and the parameters of the W3P model). The velocity recordings at Pahute Mesa are surface recordings on sediments. Using the velocity model of Leonard and Johnson [1987] and data from the shot medium (D. L. Springer, personal communication 1987), we expect an impedance amplification of about 1.4–1.6 for events at 650-m depth and about 1.8 for 1100-m depth (based on the difference between  $(\rho\alpha)^{1/2}$  at the surface and at depth). In addition the attenuation is expected to be greater for these events than for the earthquake data. To obtain an estimate for the attenuation of the *P* wave explosion data we assume a (frequency independent) value of  $Q = 50$  above 600-m depth and  $Q = 100$  for depths greater than 600 m (L. Johnson, personal communication, 1987). Events recorded at 5.0-km epicentral distances have travel times of about 1.6 s. Assuming a travel time of about 1.2 s in the  $Q = 100$  material and 0.4 s in the  $Q = 50$  material gives a total amplitude decrease of about 6.6 at 30 Hz and 1.9 at 10 Hz. There is evidence that at high frequencies, attenuation is frequency dependent; this could be expected to decrease the attenuation at 30 Hz relative to that at 10 Hz. However, the attenuation in this region is not yet well determined, so we have not attempted to correct for either attenuation or sediment amplification. Based on the assumption for  $Q$  cited above, we expect the uncorrected spectral amplitudes to approximate the source spectra at 10 Hz and underestimate it at 30 Hz.

For events Colwick, Pepato, Sheepshead, and Farm we have accelerograph recordings. These acceleration recordings are either on hard rock surface sites (stations W-17 and W-18) or from 500-m-deep boreholes (station W-9). The spectral amplitude from the borehole station was multiplied by a factor of 2 to approximate a surface recording. It is interesting to note that at the more distant (hypocentral distances from 25 to 33 km) crystalline rock surface and borehole stations the 30 Hz *P* wave energy was lost in the noise. For the event Farm, we have both hard rock accelerograph recordings (hypocentral distances approximately 21 km) and four accelerograph recordings on sediments (hypocentral distances 4–9 km). The spectral amplitudes of the recordings on sediments are approximately a factor of 2 larger at 10, 20, and 30 Hz than the more distant recordings on rock. These recordings on rock may underestimate the source amplitude due to impedance. All of the explosion data have been normalized to 10-km hypocentral distance.

#### ANALYSIS

The difference in high-frequency behavior of the W2P, W3P, and Sharpe source models as the event size increases, is illustrated in Figure 1, where spectral amplitude at 10, 20, and 30 Hz is plot-

ted versus seismic moment. The Sharpe [1942] model is represented by the dashed curve and was calculated using a maximum pressure of elastic response of 130 bars. The W2P and W3P models are represented by solid lines. The stress drop in bars associated with each curve is indicated by  $\sigma$ . The W3P curve was derived from (1) and (4) assuming the rupture velocity is equal to the shear wave velocity. The data have all been normalized to 10-km hypocentral distance and, as discussed in the introduction, not corrected for  $Q$ .

The theoretical curves all show spectral amplitude increasing linearly with moment up to about  $10^{19}$ – $10^{20}$  dyn cm. This is expected for any source model, since for these small-moment events the wavelength at the frequency of interest (10, 20, or 30 Hz) is large compared with the source dimension. In other words, these small events have corner frequencies higher than the frequency being plotted, so the spectral amplitude scales directly with moment. For the larger-moment (above about  $10^{20}$  dyn cm) events the W3P model predicts the spectral amplitudes will remain constant for a constant stress drop. The W2P model in contrast predicts for these large-moment events that the spectral amplitudes will increase with moment approximately as  $M_0^{1/3}$  for constant stress drop. The Sharpe curve has similar scaling to the W2P model.

Figure 1a shows 10-Hz spectral amplitude versus moment. The Oaxaca events show more 10-Hz energy than Anza events of comparable moment and thus could be interpreted as having higher stress drops than the Anza events in either the W2P or W3P models. However, the two models give different absolute values for stress drops. For example, the largest moment Anza events would be interpreted as having a stress drop of about 10 bars in the W2P model, while the W3P model would give stress drops of about 400 bars. Many of the Oaxaca events have as much or more 10-Hz energy than the Sharpe curve. The explosion points scatter about the Sharpe curve with the recordings on rock having less 10-Hz energy than predicted by the model. The six points representing the five small, 75–150 kt, events (Farm was recorded both on rock and sediments) have about an order of magnitude range in 10-Hz amplitude.

As we look at higher frequencies (20 Hz in Figure 1b and 30 Hz in Figure 1c) the difference in the predicted spectral amplitude of the W2P and W3P models for large-moment events becomes more pronounced. The earthquake data (Anza, Oaxaca, Mammoth, and Michoacan) show a clear increase in spectral amplitude with moment, approximately in agreement with the W2P model, and in disagreement with a constant stress drop W3P model for the larger events. If we were to interpret the data with the W3P model, stress drop would have to increase significantly with moment. For the largest moment events such as the Michoacan main shock (Figure 1c) the W3P model implies a stress drop of the order of a kilobar. This is in distinct disagreement with static stress, apparent stress, and dynamic stress as calculated by Anderson et al. [1986] and Priestley and Masters [1986] of about 5–20 bars.

The NTS explosions show increasing scatter as we look at the higher frequencies (Figures 1b and 1c). The hard rock recordings and the Farm accelerograph recording on sediments have lower spectral amplitudes at 30 Hz (Figure 1c) by 1–2 orders of magnitude. One possible explanation for this is source depth. The higher spectral amplitude events are deeper (800–1100 m) than the lower spectral amplitude events (630–690 m). The average depth to the water table in Pahute Mesa is about 650 m [Leonard and Johnson, 1987]. Events below the water table might be expected to couple more high-frequency energy into seismic waves. The majority of

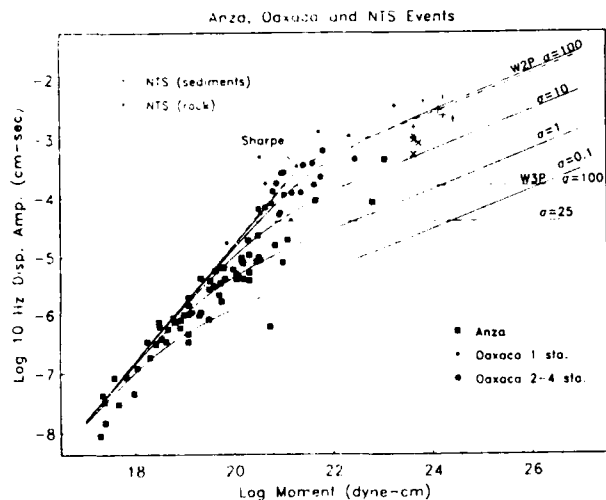


Fig. 1a

Fig. 1.  $P$  wave displacement spectral observations of earthquakes (solid symbols) and NTS explosions plotted as a function of moment, and compared with theoretical curves. All symbols and curves normalized to a hypocentral distance of 10 km. No attenuation correction was applied to the data. Events where more than one station recording was used have relatively larger symbol size. Theoretical curves given for constant stress drop denoted by  $\sigma$  in bars. W3P model given for constant rupture velocity equal to the shear wave velocity. The Sharpe curve was calculated assuming a maximum pressure of 130 bars and is indicated by the dashed curve. (a) The 10-Hz  $P$  wave displacement versus moment, (b) 20-Hz  $P$  wave displacement spectral amplitude versus moment, and (c) 30-Hz  $P$  wave displacement spectral amplitude versus moment. Note the increase in spectral amplitude with moment approximately in agreement with a constant stress drop W2P ( $\omega^{-2}$  falloff beyond the corner frequency) model and for larger moments in disagreement with the W3P ( $\omega^{-3}$  falloff beyond the corner frequency) model. Also note the explosion spectral amplitudes generally fall below the Sharpe curve.

the explosion data points have less 30-Hz energy than the Sharpe model predicts and fall in the region of the earthquake population.

### DISCUSSION

Evernden *et al.*, [1986] argue that the Sharpe model is a conservative or minimum estimate for the high-frequency energy radiated by explosions. They expect all explosion data to plot on or above this curve. The reason for the failure of all the explosion data to plot on or above the Sharpe curve may be due to loss of high frequency energy in the transmission from source to receiver, in the source spectrum itself, or some combination of both. The transmission characteristics of the medium at these high frequencies are not known well enough to determine the magnitude of this effect. Ideally a series of small nuclear explosions in hard rock recorded in hard rock would be the best comparison with the earthquake data presented here. Since these data are not available, we will be confined to making some general remarks about explosion models.

The corner frequency and falloff at high frequencies of explosion spectra are critical to the Evernden *et al.* discrimination proposal. The question of whether the step function in pressure Sharpe model represents a minimum estimate of the high-frequency energy radiated by explosions must be examined in light of the data presented. It is not clear, particularly for tamped explosions at shallow depths and high frequencies, that the pres-

sure at the elastic radius is a step function. The nonlinear processes such as crushing and plastic deformation might be expected to preferentially attenuate the high-frequency components of the pressure function. Thus it seems possible that a tamped explosion could have a spectral falloff steeper than  $\omega^{-2}$  and have less energy at high frequencies than the Sharpe model predicts. Much more work needs to be done in determining the exact high-frequency behavior of both tamped and decoupled explosions.

Figure 1 implies two important problems for high-frequency discrimination regardless of the actual attenuation. First, the high stress drop earthquakes such as some of the Oaxaca aftershocks fall close to or above the Sharpe curve. In fact both the W2P and W3P models predict that high stress drop earthquakes can radiate more high-frequency energy than the Sharpe model. Thus the question for discrimination is not only whether the W2P or W3P better describe the data but also whether high stress drop earthquakes are expected in the regions of interest and whether they can be discriminated by methods other than high-frequency spectral amplitude.

Second, it may be possible to defeat any high-frequency

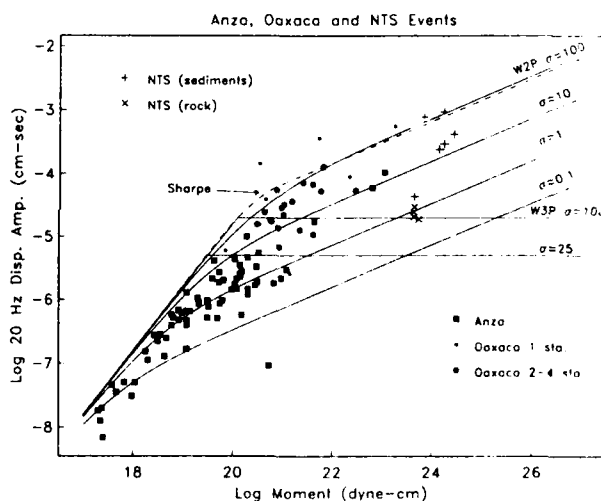


Fig. 1b

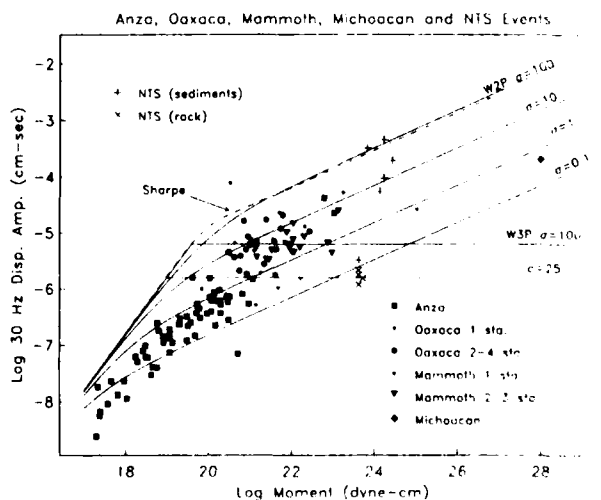


Fig. 1c

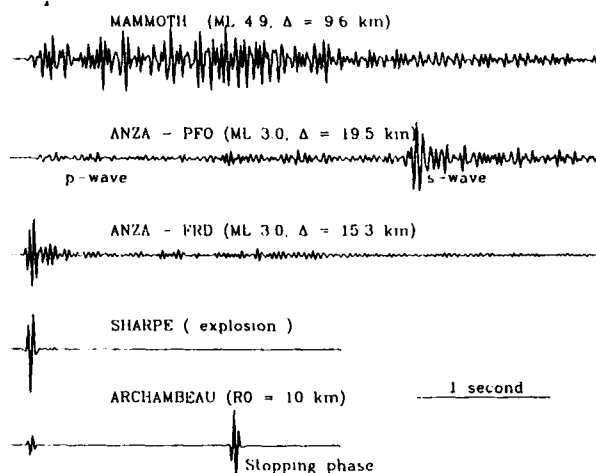


Fig. 2. Observed and theoretical velocity seismograms passed through a narrow-band filter centered at 30 Hz (20–40 Hz). The Mammoth trace represents a complex earthquake. The two Anza traces represent a single earthquake, showing simple explosionlike earthquake signal at one station (FRD) and a more typical simple seismogram with a large S wave pulse at another station (PFO). The trace for the Sharpe explosion model has all the higher-frequency energy arriving in the impulsive beginning, whereas for the W3P model the amplitude of the stopping phase is about 3 times larger than the starting phase. For the constant rupture velocity and stress drop W3P model, the 30-Hz spectrum does not increase with moment beyond  $10^{20}$  dyn cm because the pulses seen through a narrow-band filter only spread out in time, but do not change amplitude.

discrimination technique by detonating the shot in a medium with high attenuation such as is expected at Pahute Mesa. Certainly any technique based on simple spectral amplitude at 30 Hz would fail for some of the recordings of the explosion data presented here, even for events recorded as close as 5 km. Scattering and attenuation can be expected to have a larger effect on the source spectrum at these high frequencies.

The data in Figure 1c show that large earthquakes radiate more 30-Hz energy than small ones, in contrast with a constant stress drop W3P model. This is obvious from a cursory observation of the long-duration, higher-amplitude P waves from larger events. As a simple illustration of this point, we present in Figure 2, narrow-band filtered velocity seismograms (bandwidth 20–40 Hz) from three earthquake recordings along with filtered seismograms of the Sharpe explosion model and the W3P [Archambeau, 1968, 1972] earthquake model. These records clearly indicate the greater amount of 30-Hz energy radiated from larger events due to both larger peak amplitudes and longer, more complex time functions. In contrast the W3P model in Figure 2 does not radiate any more energy at 30 Hz as the moment increases, since increasing the source size only causes the starting and stopping phases of the W3P model to separate further in time, but does not change their amplitude.

The difference in the time domain of the theoretical models suggests that the waveforms themselves be considered in any high-frequency discrimination technique. The high-frequency energy radiated by earthquakes is generated by rupture complexity which can be modeled by accelerations and decelerations of the rupture front [e.g., Bernard and Madariaga, 1984]. The W3P model, as indicated in Figure 2, radiates high-frequency energy in a starting and stopping phase with the latter having about 3 times higher amplitude than the former. Explosions, in contrast, are expected to radiate high-frequency energy in an initial impulse, as indicated by the Sharpe model in Figure 2. In some cases, earth-

quake records show an impulsive "explosionlike" record at one or two stations of an array, but in these cases, the other stations of the array usually show a less impulsive, more "earthquake-like" signals with large S waves (Figure 2). There may be a problem, however, in applying such time domain or phase characteristic approach to high stress drop earthquakes. High stress drop earthquakes have high corner frequencies and smaller source dimensions and thus shorter rupture times. A magnitude 3 or 4 earthquake with a stress drop of 100 bars or more might have a rupture duration of less than a tenth of a second, and might make discrimination based on either waveform in the time domain or spectral amplitude difficult.

## CONCLUSIONS

Observations of high-frequency P wave spectra from earthquakes, normalized to a distance of 10 km, show an increase in spectral amplitude with moment approximately in agreement with an  $\omega^{-2}$  falloff model, and for large moments in disagreement with an  $\omega^{-3}$  falloff model. The explosion data at a frequency of 30 Hz generally fall below the Sharpe curve, show much scatter, and do not all discriminate from the earthquake data on the basis of spectral amplitude. How much of this effect is due to attenuation requires further investigation. This suggests that any discrimination technique using high-frequency P waves should also take into account phase information (e.g., time domain character), not just spectral level. High stress drop earthquakes can radiate more high-frequency energy than the Sharpe model and might be expected to make any technique based on time domain character of P waves difficult as well.

**Acknowledgments.** We wish to thank Jeff Barker of Woodward-Clyde Consultants for sending us the explosion velocity spectra, John Anderson for supplying the Michoacan data, and Linda Haar of the U.S. Geological Survey for assistance in processing the Anza data. We would also like to thank John Banister at Sandia National Laboratory for supplying the explosion accelerograms. U. C. Berkley provided accelerograph recordings for one NTS event. This research was supported by Lawrence Livermore National Laboratory under subcontract 1644503. Preliminary work by one of the authors (W.R.W.) was supported by a Sloan Foundation/IGCC Fellowship.

## REFERENCES

- Aki, K., The scaling laws of earthquake source time spectrum, *Geophys. J. R. Astron. Soc.*, **31**, 3–25, 1972.
- Anderson, J. G., P. Bodin, J. N. Brune, J. Prince, S. K. Singh, R. Quaas, and M. Onate, Strong ground motion from the Michoacan, Mexico, earthquake, *Science*, **233**, 1043–1049, 1986.
- Archambeau, C. B., General theory of elastodynamic source fields, *Rev. Geophys.*, **6**, 241–288, 1968.
- Archambeau, C. B., The theory of stress wave radiation from explosions in prestressed media, *Geophys. J.*, **29**, 329–366, 1972.
- Archambeau, C. B., and J. B. Minster, Dynamics in prestressed media with moving boundaries: A continuum theory of failure of solids, *Geophys. J. R. Astron. Soc.*, **29**, 65–96, 1978.
- Archuleta, R. J. and G. A. Frazier, Three-dimensional numerical simulations of dynamic faulting in a half space, *Bull. Seismol. Soc. Am.*, **68**, 541–572, 1978.
- Archuleta, R. J., E. Cranswick, C. Mueller, and P. Spudich, Source parameters of the 1980 Mammoth Lakes, California, earthquake sequence, *J. Geophys. Res.*, **87**, 4559–4585, 1982.
- Barker, J. S., L. J. Burdick, and T. C. Wallace, Analysis of near-field seismic waveforms from underground nuclear explosions, *Final Technical Report AFGL-TR-85-0321*, Air Force Geophys. Lab., Bedford, Mass., 1985.
- Berger, J., L. N. Baker, J. N. Brune, J. B. Fletcher, T. C. Hanks, and F. L. Vernon, The Anza array: a high dynamic-range, broad-band, digitally radio-telemetered seismic array, *Bull. Seismol. Soc. Am.*, **74**, 1469–1482, 1984.
- Bernard, P., and R. Madariaga, A new asymptotic method for the model-

- ing of near field accelerograms, *Bull. Seismol. Soc. Am.*, **74**, 539-557, 1984.
- Blandford, R. R., A source theory for complex earthquakes, *Bull. Seismol. Soc. Am.*, **65**, 1385-1405, 1975.
- Brune, J. N., Tectonic stress and the spectra of seismic shear waves from earthquakes, *J. Geophys. Res.*, **75**, 4997-5009, 1970.
- Brune, J. N., Correction, *J. Geophys. Res.*, **76**, 5002, 1971.
- Brune, J. N., R. S. Simons, F. Vernon, L. Canales, and A. Reyes, Digital seismic event recorders: description and examples from the San Jacinto fault, the Imperial fault, the Cerro Prieto fault and the Oaxaca, Mexico subduction fault, *Bull. Seismol. Soc. Am.*, **70**, 1395-1408, 1980.
- Brune, J. N., W. R. Walter, K. F. Priestley, J. Fletcher, F. Vernon, J. Berger, S. Hough, and T. Hanks, Preliminary observations of 30 Hz P-wave earthquake spectra compared with  $\omega^{-3}$  and  $\omega^{-2}$  source models, Paper presented at Conference on Research in High-Frequency Seismology, sponsored by Lawrence Livermore National Laboratory and the Defense Advanced Research Projects Agency, Dallas, Tex., 1986a.
- Brune, J. N., J. Fletcher, F. Vernon, L. Haar, T. Hanks, and J. Berger, Low stress-drop earthquakes in light of new data from the Anza, California telemetered digital array in *Earthquake Source Mechanics, Maurice Ewing Ser.*, vol. 6, edited by S. Das, J. Boatwright, and C. Schultz, pp. 237-245, AGU, Washington, D.C., 1986b.
- Evernden, J. F., C. B. Archambeau, and E. Cranswick, An evaluation of seismic decoupling and underground nuclear test monitoring using high frequency seismic data, *Rev. Geophys.*, **24**, 143-216, 1986.
- Fletcher, J., L. Haar, T. Hanks, L. Baker, F. Vernon, J. Berger, and J. Brune, The digital array at Anza, California: Processing and initial interpretation of source parameters, *J. Geophys. Res.*, **92**, 369-382, 1987.
- Frankel, A., J. Fletcher, F. Vernon, L. Haar, J. Berger, T. Hanks, and J. N. Brune, Rupture characteristics and tomographic source imaging of  $M_L \sim 3$  earthquakes near Anza, southern California, *J. Geophys. Res.*, **91**, 12,633-12,650, 1986.
- Hanks, T. C.,  $b$  values and  $\omega^{-\gamma}$  seismic source models, implications for tectonic stress variations along active crustal fault zones and the estimation for high-frequency strong ground motion, *J. Geophys. Res.*, **84**, 2235-2242, 1979.
- Hanks, T. C., The corner frequency shift, earthquake source models, and  $Q$ , *Bull. Seismol. Soc. Am.*, **71**, 597-612, 1981.
- Harr, L., J. Fletcher, H. Liu, R. Warrick, and R. Westerlund, Near surface effects at Anza: comparison of surface and borehole data (abstract), *Seism. Res. Lett.*, **58**, 26, 1987.
- Haskell, N., Total energy and energy spectral density of elastic wave radiation from propagating faults, *Bull. Seismol. Soc. Am.*, **54**, 1811-1841, 1964.
- Kanamori, H., A semi-empirical approach to the prediction of long-period ground motions from great earthquakes, *Bull. Seismol. Soc. Am.*, **69**, 1645-1670, 1979.
- Kanamori, H., and G. S. Stewart, Seismological aspects of the Guatemala earthquake of February 4, 1976, *J. Geophys. Res.*, **83**, 3427-3434, 1978.
- Keilis-Borok, V. I., On estimation of the displacement in an earthquake source and of source dimensions, *Ann. Geophys.*, **12**, 205-214, 1959.
- Latter, A. L., R. E. LeLevier, E. A. Martinelli, and W. G. McMillan, A method for concealing nuclear explosions, *J. Geophys. Res.*, **66**, 943-946, 1961.
- Leonard, M. A., and L. R. Johnson, Velocity structure of silent canyon taldera, Nevada test site, *Bull. Seismol. Soc. Am.*, **77**, 597-613, 1987.
- Minster, J. B., Elastodynamics of failure in a continuum, Ph.D. Thesis, Calif. Inst. of Technol., Pasadena, 1973.
- Minster, J. B., and A. M. Suteau, Far-field waveforms from an arbitrarily expanding, transparent spherical cavity in a prestressed medium, *Geophys. J. R. Astron. Soc.*, **50**, 215-233, 1977.
- Mueller, R. A., and J. R. Murphy, Seismic characteristics of underground nuclear detonations, Part I. Seismic spectrum scaling, *Bull. Seismol. Soc. Am.*, **61**, 1675-1692, 1971.
- Munguia, L., and J. N. Brune, Simulations of strong ground motions for earthquakes in Mexicali-Imperial Valley, *Geophys. J. R. Astron. Soc.*, **79**, 747-771, 1984.
- Munguia, L., J. N. Brune, A. Reyes, J. Gonzalez, R. Simons, and F. Vernon, Digital seismic event recorder records and spectra for aftershocks of the November 29, 1978 Oaxaca earthquake, *Geophys. Int.*, **17**, 359-366, 1978.
- Papageorgiou, A. S., and K. Aki, A specific barrier model for the quantitative description of inhomogeneous faulting and the prediction of strong ground motion, Part I, Description of the model, *Bull. Seismol. Soc. Am.*, **73**, 693-722, 1983a.
- Papageorgiou, A. S., and K. Aki, A specific barrier model for the quantitative description of inhomogeneous faulting and the prediction of strong ground motion, Part II, Applications of the model, *Bull. Seismol. Soc. Am.*, **73**, 953-978, 1983b.
- Patterson, D. W., Nuclear decoupling partial and full, *J. Geophys. Res.*, **71**, 3427-3436, 1966.
- Priestley, K. F., and G. Masters, Source mechanism of the September 19, 1985 Michoacan earthquake and its implications, *Geophys. Res. Lett.*, **13**, 601-604, 1986.
- Priestley, K. F., J. N. Brune, and J. G. Anderson, Surface wave excitation and source mechanisms of the Mammoth Lakes earthquake sequence, *J. Geophys. Res.*, **90**, 11,177-11,185, 1985.
- Reyes, A., J. Gonzalez, L. Munguia, A. Nava, F. Vernon, J. N. Brune, Locations of aftershocks of the Oaxaca earthquake using smoked paper recorders and digital event recorders, *Geophys. Int.*, **17**, 341-350, 1978.
- Sharpe, J. A., The production of elastic waves by explosion pressures, I. Theory and empirical field observations, *Geophysics*, **7**, 144-154, 1942.
- Springer, D. L., and R. L. Kinnman, Seismic source summary for U. S. underground nuclear explosions, 1961-1970, *Bull. Seismol. Soc. Am.*, **61**, 1073-1098, 1971.
- Stevens, J. L., Seismic radiation from the sudden creations of a spherical cavity in an arbitrarily prestressed medium, *Geophys. J. R. Astron. Soc.*, **61**, 303-328, 1980.
- Trifunac, M. D., and J. N. Brune, Complexity of energy release during the Imperial Valley, California, earthquake of 1940, *Bull. Seismol. Soc. Am.*, **60**, 137-160, 1970.
- Tucker, B. E., and J. N. Brune, Source mechanism and  $m_p - M_s$  analysis of aftershocks of the San Fernando earthquake, *Geophys. J. R. Astron. Soc.*, **49**, 371-426, 1977.
- Wyss, M., and J. N. Brune, The Alaska earthquake of 28 March 1964: A complex multiple rupture, *Bull. Seismol. Soc. Am.*, **57**, 1017-1023, 1967.

J. N. Brune, K. F. Priestley, and W. R. Walter, Seismological Laboratory, Mackay School of Mines, University of Nevada, Reno, NV 89557.  
J. Fletcher, U.S. Geological Survey, 345 Middlefield Road, Menlo Park, CA 94025.

(Received September 16, 1987;  
revised January 25, 1988;  
accepted January 25, 1988.)

# CRUSTAL STRUCTURE IN EASTERN KAZAKH, U.S.S.R. FROM TELESEISMIC RECEIVER FUNCTIONS

Keith F. Priestley

Seismological Laboratory, University of Nevada at Reno, Reno, NV

George Zandt, and George E. Randall

Institute of Geophysics and Planetary Physics, Lawrence Livermore National Laboratory, Livermore, Ca

**Abstract.** Broadband receiver functions determined from teleseismic P-waveforms recorded at two seismic stations in eastern Kazakh, U.S.S.R., are inverted for the vertical velocity structure beneath the stations. The detailed broadband receiver functions are obtained by stacking source-equalized radial components of teleseismic P-waveforms. A time-domain inversion of the radial receiver function is used to determine the structure assuming a crustal model parameterized by flat-lying, homogeneous layers. The general features of the inversion results are: a complex shallow crust, velocities less than 6 km/s in the upper crust, a high velocity (6.9-7.5 km/s) lower crust, and a Moho that varies between 47 and 57 km depth. These results compare favorably with a composite velocity model from Deep Seismic Sounding data, but show lower velocities in the upper crust, and higher velocities in the lower crust. The results indicate that the crust in this region is relatively uniform, however the nature and depth of the Moho changes significantly across the region. The receiver function inversion structure for the Kazakh sites is similar to a published receiver function structure for a site on the Canadian Shield.

## Introduction

Since July, 1986 three seismic stations have been operating in the vicinity of the Soviet nuclear test site in eastern Kazakh, U.S.S.R., under a joint agreement between the Natural Resources Defense Council (NRDC) and the Soviet Academy of Science [Berger et al, 1987]. Data from July, 1986, through February, 1987 were from seismometers placed in surface vaults; since March, 1987, data also have been recorded from seismometers located in 100 meter deep boreholes beneath the surface vaults. All data are digitally recorded. Figure 1 shows the location of the three stations (KKL, BAY, KSU), the locations of teleseismic earthquakes used in this study, and the Deep Seismic Sounding (DSS) line discussed by Antonenko [1984].

Leith [written communications, 1987] has compiled geophysical and geological data for the NRDC sites, from the Soviet literature. The seismograph sites lie within the Kazakh fold system, a belt of folded and faulted Paleozoic rocks. The region was marked by extensive igneous

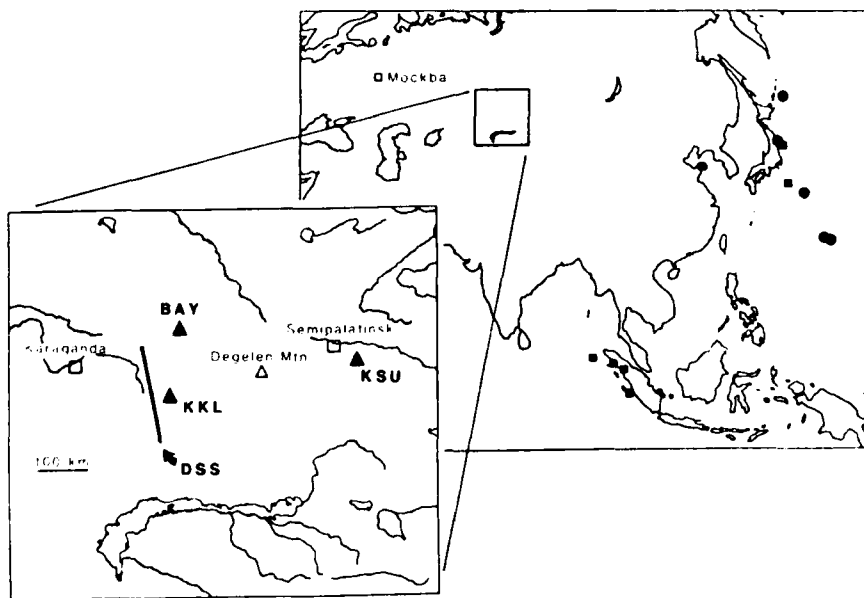


Fig. 1. The lower part of the figure shows the location of the NRDC seismic stations, Degelen Mountain on the Soviet test site, and the DSS line discussed by Antonenko (1984). The upper part of the figure shows the location of the study area in central Asia, and the location of the teleseismic events studied: (■) denote events recorded at KKL, (●) denote events recorded at BAY.

Copyright 1988 by the American Geophysical Union.

Paper number 8L7319.  
0094-8276/88/008L-7319\$03.00

activity during the late stages of the Hercynian Orogeny during the Permo-Triassic Period. The three seismograph sites are located on small granitic intrusions of Paleozoic to early Mesozoic age. The granites were intruded into deformed Paleozoic sedimentary rocks. Subsequent tectonic activity has resulted in regional crustal uplift and thickening. Leith [un-



gests that the geological and geophysical characteristics of Degelen Mountain on the Soviet Test Site are similar to those of the Karkaralinsk and Bayanaul intrusions. The plutons and Degelen Mountain are composed of alaskite, an alkali feldspar granite of slightly lower density and seismic velocity than typical granite. Based on Soviet deep seismic sounding lines in the area, the Pn-velocity appears to vary from 8.0 to 8.3 km/s and the crustal thickness varies from 50 km in the vicinity of Karkaralinsk and Bayanaul to possibly as little as 40 km at Karasu. Soviet geophysical results indicate that at least the Karkaralinsk intrusion is a laccolith narrowing from an area of about 450 km<sup>2</sup> at the surface to about 100 km<sup>2</sup> at a depth of 10 km.

In this report, we model receiver functions obtained from teleseismic P-waveforms recorded at two sites, Karkaralinsk and Bayanaul, to determine the detailed structure of the crust and upper mantle directly beneath the recording site. Insufficient data has been recorded from the Karasu site for this type of analysis. The broadband receiver function method is most sensitive to the details of the vertical shear velocity distribution in the crust, a difficult parameter to constrain using other methods. We estimate gross lateral variations in structure by examining the variation in vertical velocity distribution azimuthally around the station, and by examining the relative magnitude of the transverse and radial arrivals. Finally, assuming a constant Poisson's ratio we compare our results with P-velocity profiles from a nearby DSS line.

#### Data and Analysis

We have used the deconvolution procedure proposed by Langston [1979] to isolate the response of the structure beneath the seismograph (the receiver function) from the source and path effects, all of which interact to form the observed seismograms recorded at teleseismic distances. For teleseisms recorded at 30° to 90° epicentral distance, the initial energy arriving from the source region consists of plane P-wave arrivals. Since the earth structure beneath the station will produce P to S conversions the horizontal component of ground motion will in general be quite different from the vertical component. Langston [1979] has shown that the receiver function can be obtained by deconvolving the vertical component from the radial. The resulting receiver functions from events clustered both in distance and back azimuth are then stacked in the time domain to obtain a single estimate of the horizontal receiver function. Stacking the deconvolved traces from individual events averages small differences in the estimated mean receiver functions and improves the signal-to-noise ratios.

Figure 2 shows seismograms recorded at KKL from shallow and deep focus events in Japan. The upper three traces are the vertical, radial and transverse components, respectively. The recorded seismograms show the

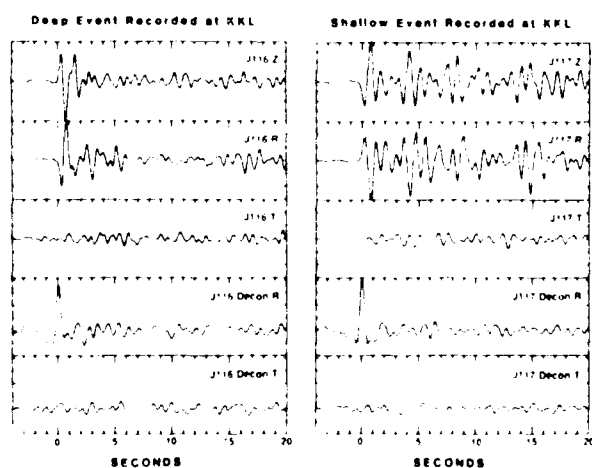


Fig. 2. Deep and shallow focus events recorded at KKL. The upper three traces are the vertical, radial, and transverse components, respectively. The lower two traces are the deconvolved radial and transverse receiver functions. The horizontal components are plotted at the same scale.

differences in complexity typically seen between deep and shallow focus events. The bottom two traces are the deconvolved radial and transverse components. The deconvolved radial components for both events show very similar features, although these two traces exhibit the largest differences among individual seismograms used in any of the three stacks reported in this paper. The seismograms available were sufficient to produce three stacked receiver functions: Two for separate azimuths for KKL and one for BAY. The stack for KKL-Japan includes three events; the stack for KKL-Sumatra has 4 events; and the BAY-Japan stack has 6 events. The stacked radial receiver functions tend to decay rapidly in amplitude, indicating a relatively homogeneous crust. The transverse components are generally small and have nearly constant amplitude, indicating that lateral variations in the structure are small.

The stacked receiver functions were inverted using a standard, linearized inversion procedure [Owens et al., 1984] with the modified fast partial derivatives method of Randall [1988]. The earth structure is parameterized by a series of plane horizontal layers, and an iterative procedure is used to minimize the residual difference between the radial receiver function and the synthetic predicted by the structure. Our starting model for the KKL and BAY inversions is from the structure compiled by Leith [written communications, 1987] from the Soviet DSS literature. The inversion model is parameterized with 1.0 km thick layers in the shallow crust (upper 5 km), and 2.5 km thick layers to a depth of 57.5 km. We invert for the vertical shear wave velocity structure for each back azimuth for which we had sufficient data; the compressional velocities are obtained by assuming a Poisson's ratio of 0.25, and the densities are obtained using the relationship  $\rho = 0.32 V_p + 0.77$  [Owens et al., 1984]. The variation in structure with azimuth allows a qualitative estimate of the lateral variation in structure about the station. The results from the thin-layer inversions were examined to identify the depths of the significant seismic impedance contrasts, then the models were reparameterized with thicker layers and

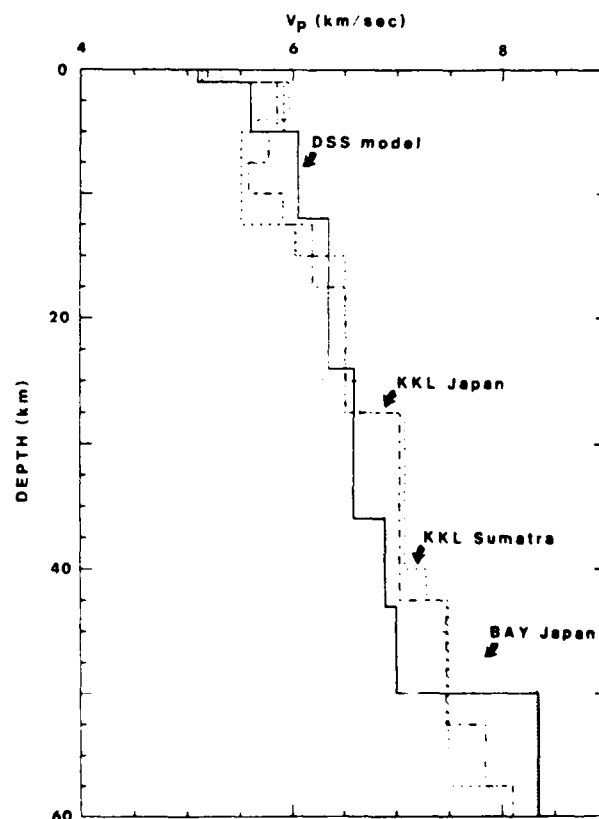


Fig. 3. Comparison of the starting model and final inversion results. The inversion results are in terms of the shear wave structure, however for comparison with the DSS results, the models are presented as compressional wave velocity assuming a Poisson's ratio of 0.25.

Table 1. Final Velocity Models

Leith h a	BAY-Japan h a	KKL-Japan h a	KKL-Sumatra h a
1.0 5.10	1.0 5.32	1.0 5.19	1.0 5.14
4.0 5.60	3.0 5.96	4.0 5.85	4.0 5.91
7.0 6.05	6.0 5.66	2.5 5.77	7.5 5.51
12.0 6.35	5.0 6.01	2.5 5.57	2.5 6.03
12.0 6.60	10.0 6.29	2.5 5.90	12.5 6.51
7.0 6.90	5.0 6.65	5.0 6.19	12.5 7.08
7.0 7.00	15.0 6.89	10.0 6.52	2.5 7.29
∞ 8.35	2.5 7.59	15.0 7.04	15.0 7.49
	∞ 8.33	10.0 7.47	∞ 8.10
		5.0 7.80	
		∞ 8.10	

h = layer thickness in km, a = P-velocity in km/s

inverted again. All the inversions used in this study converged and final results included all singular values; hence the model resolution is theoretically perfect. We attempted to determine final models with the minimum number of parameters to obtain a satisfactory fit to the data.

### Results

The final inversion velocity models are shown in Figure 3 and tabulated in Table 1. The models are shown in terms of the P-wave velocity structure, assuming a Poisson's ratio of 0.25. Leith's summary of the DSS results, which was used as a starting model for the inversions, is shown as the solid line. Two models are shown for KKL, one for data from Japan earthquakes and one from Sumatra earthquakes. The  $2\sigma$  error bounds varied with depth but averaged about 0.1 km/s, however the differences between the two KKL models may be more representative of the model variance. A single BAY structure is shown for data from Japan earthquakes.

The data from the three stacks were inverted separately with a model parameterized by thin layers and using the Leith starting model. The resulting inversion models have a complex shallow crust with thin high-velocity layers. The upper few kilometers of the structures are complicated by the laccolith intrusions and thus may be expected to deviate from the plane layered structure assumed. Also, pronounced side lobes about the main arrival (see Figure 2) result from deconvolution of the band-limited data (the synthetic seismograms were treated in the same manner), and some of the complexity in the shallow crust results from the inversion trying to fit this artifact. To assess the effect of this in the deeper structure we have recomputed the synthetics with a smoother shallow crust and thicker layer parameters, as we described earlier. The subsequent synthetics still fit the lower frequency component of the data, indicating that the overall features of the structure are not biased by the complexities in the shallow crust.

The overall features of the two KKL models for data from two azimuths about  $75^\circ$  apart are the same, implying no pronounced systematic nonplanar structure. This is supported by the small signals in the deconvolved tangential components (Fig. 2). Compared with the summary of the DSS data from Leith, velocities in the upper crust (5-15 km depth) are slower, less than 6 km/s. The velocity model from inversion of the KKL receiver function is faster in the lower crust compared to the DSS model, with velocities reaching 7 km/s at depths as shallow as 27.5 km as opposed to 36 km depth in the DSS model. The most significant difference is in the nature of the Moho. The DSS model has a very pronounced Moho at 50 km depth, whereas the receiver function models have a much less distinct Moho at 52-57 km. The upper two traces of Figure 4 show the fits of the synthetic radial receiver functions calculated for the two KKL models of Figure 3, overplotted on the radial receiver function stacks. The fits for the thin layer inversions were much better, however we did not feel justified in fitting the data to that extent, and feel the coarser models shown in Figure 3 are more realistic.

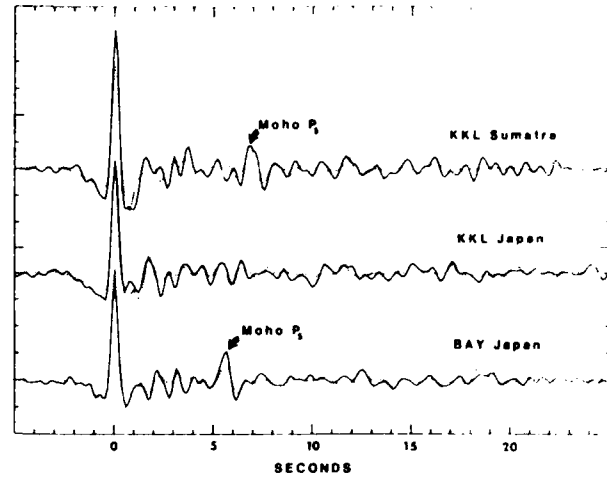


Fig. 4. Fit of synthetic receiver functions (dotted lines) and the observed (solid lines) stacked radial receiver functions. Top traces for KKL Sumatra, middle for KKL Japan, and bottom for BAY Japan.

The result for the BAY-Japan inversion is also shown in Figure 3 and tabulated in Table 1, and the fit of the synthetic to the stack is shown in Figure 4. In general the features of the BAY model are similar to those for KKL: a complex shallow crust, an upper crustal low velocity zone and a mid-crustal interface near 15 km; however the lower crustal velocities are generally slower and the Moho is both shallower and more distinct than observed at KKL. In fact, below 10 km the BAY velocity structure is quite close to the DSS velocity structure except the Moho is shallower (45 - 47.5 km depth) than in the DSS model (50 km). Although we have only inverted BAY data from one azimuth, the small signal observed on the deconvolved tangential component relative to the radial implies that the structure does not depart systematically from the assumed horizontal layers.

The largest differences among all three inversion models are in the depth and nature of the Moho. The Moho from the KKL-Japan inversion is less pronounced than that from the KKL-Sumatra inversion. The relatively strong arrival in the KKL-Sumatra stack at 7 sec is predominantly the Moho P-to-S conversion and is the controlling factor for the depth and impedance contrast of that interface. The arrival is weak or missing in the KKL-Japan stack. This azimuthal variation may reflect variations in the amplitude of a converted phase from a dipping layer or the interference between multiple arrivals which can be easily destroyed by lateral variations in velocity or layer thickness. The lack of corresponding systematic arrivals on the transverse component favors the interference explanation; also the Soviet DSS studies in the region indicate significant lateral variations in the Moho. The prominent Ps phase in the BAY-Japan stack at 5.5 seconds controls the shallower depth and larger contrast of the Moho on the BAY model. Zandt and Owens [1986] discussed a similar comparison between refraction and receiver function derived velocity structures at the Cumberland Plateau, eastern Tennessee. The more distinct nature of the refraction Moho compared with the receiver function Moho observed in both studies most likely results from differences in the frequency and phase velocities of the arrivals utilized by the two techniques.

### Summary and Conclusions

Teleseismic receiver functions from broadband waveforms recorded in eastern Kazakh have been inverted for the crustal velocity structure and compared with a summary of DSS data compiled by Leith. The results are summarized in terms of P-wave velocity models in Table 1 and plotted in Figure 3. Our results are in general agreement with the DSS data, although our models indicate the presence of a high velocity (> 8 km/s) layer below 30 km which is not seen in the DSS results. This represents either real differences in velocity or variations in Poisson's ratio. The inversion structures from data recorded at the two sites, which are approximately 150 km apart, are similar indicating that the crust in this region

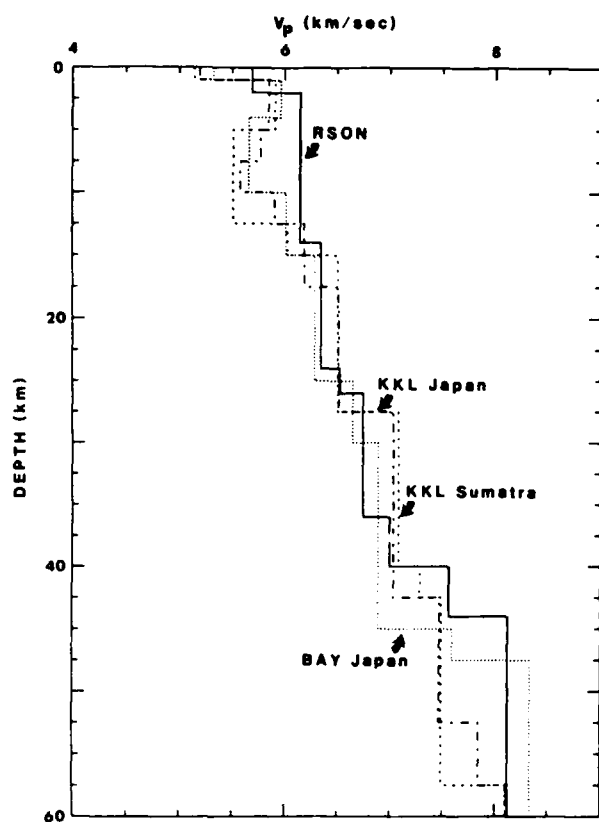


Fig. 5. Comparison of the Kazakh receiver function inversion models with the receiver function inversion model of Owens et al (1987) for the RSON site on the Canadian Shield.

may be relatively uniform. However, the nature of the Moho is different between the two sites; at Bayanaul it is shallower (47 km depth) and much more distinct than at Karkaralinsk (52-57 km depth). The shallow crust is complex, showing thin high velocity layers above an upper crustal low velocity zone. These shallow features may not be regional, but may be largely confined to the laccoliths in which the seismic stations are sited.

In Figure 5 the Bayanaul and Karkaralinsk receiver function models are compared with a smoothed receiver function model for Red Lake, Ontario (RSON) on the Canadian Shield [Owens et al, 1987]. Studies of data from RSON have often been used as analogs for the Kazakh region of the Soviet Union. The shallow crust at RSON has higher velocities than our Kazakh models, however this may be from complexities introduced from the Kazakh stations being sited in the laccolith intrusions, whereas RSON

is located on a more uniform upper crust. Also, the Kazakh sites are located in alaskite granitic intrusions which have lower velocity than the metasedimentary- gneiss terrain where RSON is sited. Between 10 and 40 km depth the Kazakh and RSON models are nearly identical. The RSON model has a somewhat lower velocity in the lower crust (26 to 36 km depth), but has a shallower Moho (40 to 45 km depth) than observed for Kazakh.

**Acknowledgments.** KFP was supported by LLNL grant 1644503 and NSF grant EAR8708506. This work was performed under the auspices of the U.S. Department of Energy by the Lawrence Livermore National Laboratory under contract number (W-7405-ENG-48). We thank W. Leith for a preprint of his report prior to publication. We thank Steve Jarpe and Steve Taylor for reviewing the manuscript.

#### References

- Antonenko, A.N., *Glubinaya struktura zemnoy kori Kazakhstana*, Nauka, Alma-Ata, 122-130, 1984.
- Berger, J., J.N. Brune, P.A. Bodin, J.S. Gombert, D.M. Carrel, K.F. Priestley, D.E. Chavez, W.R. Walter, C.B. Archambeau, T.B. Cochran, I.L. Nersisov, M.B. Gokhberg, O.A. Stolyrov, S. K. Daragan, N.D. Tarassov, and Y. A. Sutelov, A new U.S.-U.S.S.R. Seismological Program, *EOS*, 68, 105-109, 1987.
- Langston, C.A., Structure under Mount Rainier, Washington, inferred from teleseismic body waves, *J. Geophys. Res.*, 84, 4749-4762, 1979.
- Owens, T.J., G. Zandt, and S.R. Taylor, Seismic evidence for an ancient rift beneath the Cumberland Plateau, Tennessee: A detailed analysis of broadband teleseismic P waveforms, *J. Geophys. Res.*, 89, 7783-7795, 1984.
- Owens, T.J., S.R. Taylor, and G. Zandt, Crustal structure at regional seismic test network stations determined from inversion of broadband teleseismic P waveforms, *Bull. Seism. Soc. Am.*, 77, 631-662, 1987.
- Randall, G.E., Efficient calculation of differential seismograms for lithospheric receiver functions, submitted to *Geophys. J. R. astron. Soc.*, 1988.
- Zandt, G., and T.J. Owens, Comparison of crustal velocity profiles determined by seismic refraction and teleseismic methods, *Tectonophysics*, 128, 155-162, 1986.

Keith F. Priestley, Seismological Laboratory, Mackay School of Mines, University of Nevada-Reno, Reno, NV 89557.

George E. Randall, and George Zandt, Institute of Geophysics and Planetary Physics, L-202, Lawrence Livermore National Laboratory, P.O. Box 808, Livermore, Ca. 94550.

(Received February 16, 1988;

Accepted March 23, 1988.)

CONTRACTORS (United States)

Prof. Thomas Ahrens  
Seismological Lab, 252-21  
Division of Geological & Planetary Sciences  
California Institute of Technology  
Pasadena, CA 91125

Prof. Charles B. Archambeau  
CIRES  
University of Colorado  
Boulder, CO 80309

Prof. Muawia Barazangi  
Institute for the Study of the Continent  
Cornell University  
Ithaca, NY 14853

Dr. Douglas R. Baumgardt  
ENSCO, Inc  
5400 Port Royal Road  
Springfield, VA 22151-2388

Prof. Jonathan Berger  
IGPP, A-025  
Scripps Institution of Oceanography  
University of California, San Diego  
La Jolla, CA 92093

Dr. Lawrence J. Burdick  
Woodward-Clyde Consultants  
566 El Dorado Street  
Pasadena, CA 91109-3245

Dr. Karl Coyner  
New England Research, Inc.  
76 Olcott Drive  
White River Junction, VT 05001

Prof. Vernon F. Cormier  
Department of Geology & Geophysics  
U-45, Room 207  
The University of Connecticut  
Storrs, CT 06268

Prof. Steven Day  
Department of Geological Sciences  
San Diego State University  
San Diego, CA 92182

Dr. Zoltan A. Der  
ENSCO, Inc.  
5400 Port Royal Road  
Springfield, VA 22151-2388

Prof. John Ferguson  
Center for Lithospheric Studies  
The University of Texas at Dallas  
P.O. Box 830688  
Richardson, TX 75083-0688

Prof. Stanley Flatte  
Applied Sciences Building  
University of California  
Santa Cruz, CA 95064

Dr. Alexander Florence  
SRI International  
333 Ravenswood Avenue  
Menlo Park, CA 94025-3493

Prof. Henry L. Gray  
Vice Provost and Dean  
Department of Statistical Sciences  
Southern Methodist University  
Dallas, TX 75275

Dr. Indra Gupta  
Teledyne Geotech  
314 Montgomery Street  
Alexandria, VA 22314

Prof. David G. Harkrider  
Seismological Laboratory  
Division of Geological & Planetary Sciences  
California Institute of Technology  
Pasadena, CA 91125

Prof. Donald V. Helmberger  
Seismological Laboratory  
Division of Geological & Planetary Sciences  
California Institute of Technology  
Pasadena, CA 91125

Prof. Eugene Herrin  
Institute for the Study of Earth and Man  
Geophysical Laboratory  
Southern Methodist University  
Dallas, TX 75275

Prof. Robert B. Herrmann  
Department of Earth & Atmospheric Sciences  
St. Louis University  
St. Louis, MO 63156

Prof. Bryan Isacks  
Cornell University  
Department of Geological Sciences  
SNEE Hall  
Ithaca, NY 14850

Dr. Rong-Song Jih  
Teledyne Geotech  
314 Montgomery Street  
Alexandria, VA 22314

Prof. Lane R. Johnson  
Seismographic Station  
University of California  
Berkeley, CA 94720

Prof. Alan Kafka  
Department of Geology & Geophysics  
Boston College  
Chestnut Hill, MA 02167

Prof. Fred K. Lamb  
University of Illinois at Urbana-Champaign  
Department of Physics  
1110 West Green Street  
Urbana, IL 61801

Prof. Charles A. Langston  
Geosciences Department  
403 Deike Building  
The Pennsylvania State University  
University Park, PA 16802

Professor Thorne Lay  
Institute of Tectonics  
Earth Science Board  
University of California, Santa Cruz  
Santa Cruz, CA 95064

Prof. Arthur Lerner-Lam  
Lamont-Doherty Geological Observatory  
of Columbia University  
Palisades, NY 10964

Dr. Christopher Lynnes  
Teledyne Geotech  
314 Montgomery Street  
Alexandria, VA 22314

Prof. Peter Malin  
University of California at Santa Barbara  
Institute for Crustal Studies  
Santa Barbara, CA 93106

Dr. Randolph Martin, III  
New England Research, Inc.  
76 Olcott Drive  
White River Junction, VT 05001

Dr. Gary McCartor  
Mission Research Corporation  
735 State Street  
P.O. Drawer 719  
Santa Barbara, CA 93102 (2 copies)

Prof. Thomas V. McEvilly  
Seismographic Station  
University of California  
Berkeley, CA 94720

Dr. Keith L. McLaughlin  
S-CUBED  
A Division of Maxwell Laboratory  
P.O. Box 1620  
La Jolla, CA 92038-1620

Prof. William Menke  
Lamont-Doherty Geological Observatory  
of Columbia University  
Palisades, NY 10964

Stephen Miller  
SRI International  
333 Ravenswood Avenue  
Box AF 116  
Menlo Park, CA 94025-3493

Prof. Bernard Minster  
IGPP, A-025  
Scripps Institute of Oceanography  
University of California, San Diego  
La Jolla, CA 92093

Prof. Brian J. Mitchell  
Department of Earth & Atmospheric Sciences  
St. Louis University  
St. Louis, MO 63156

Mr. Jack Murphy  
S-CUBED, A Division of Maxwell Laboratory  
11800 Sunrise Valley Drive  
Suite 1212  
Reston, VA 22091 (2 copies)

Dr. Bao Nguyen  
GL/LWH  
Hanscom AFB, MA 01731-5000

Prof. John A. Orcutt  
IGPP, A-025  
Scripps Institute of Oceanography  
University of California, San Diego  
La Jolla, CA 92093

Prof. Keith Priestley  
University of Nevada  
Mackay School of Mines  
Reno, NV 89557

Prof. Paul G. Richards  
Lamont-Doherty Geological Observatory  
of Columbia University  
Palisades, NY 10964

Dr. Wilmer Rivers  
Teledyne Geotech  
314 Montgomery Street  
Alexandria, VA 22314

Dr. Alan S. Ryall, Jr.  
Center for Seismic Studies  
1300 North 17th Street  
Suite 1450  
Arlington, VA 22209-2308

Prof. Charles G. Sammis  
Center for Earth Sciences  
University of Southern California  
University Park  
Los Angeles, CA 90089-0741

Prof. Christopher H. Scholz  
Lamont-Doherty Geological Observatory  
of Columbia University  
Palisades, NY 10964

Prof. David G. Simpson  
Lamont-Doherty Geological Observatory  
of Columbia University  
Palisades, NY 10964

Dr. Jeffrey Stevens  
S-CUBED  
A Division of Maxwell Laboratory  
P.O. Box 1620  
La Jolla, CA 92038-1620

Prof. Brian Stump  
Institute for the Study of Earth & Man  
Geophysical Laboratory  
Southern Methodist University  
Dallas, TX 75275

Prof. Jeremiah Sullivan  
University of Illinois at Urbana-Champaign  
Department of Physics  
1110 West Green Street  
Urbana, IL 61801

Prof. Clifford Thurber  
University of Wisconsin-Madison  
Department of Geology & Geophysics  
1215 West Dayton Street  
Madison, WI 53706

Prof. M. Nafi Toksoz  
Earth Resources Lab  
Massachusetts Institute of Technology  
42 Carleton Street  
Cambridge, MA 02142

Prof. John E. Vidale  
University of California at Santa Cruz  
Seismological Laboratory  
Santa Cruz, CA 95064

Prof. Terry C. Wallace  
Department of Geosciences  
Building #77  
University of Arizona  
Tucson, AZ 85721

Dr. Raymond Willeman  
GL/LWH  
Hanscom AFB, MA 01731-5000

Dr. Lorraine Wolf  
GL/LWH  
Hanscom AFB, MA 01731-5000

Prof. Francis T. Wu  
Department of Geological Sciences  
State University of New York  
at Binghamton  
Vestal, NY 13901

Dr. Richard LaCoss  
MIT-Lincoln Laboratory  
M-200B  
P. O. Box 73  
Lexington, MA 02173-0073

OTHERS (United States)

Dr. Monem Abdel-Gawad  
Rockwell International Science Center  
1049 Camino Dos Rios  
Thousand Oaks, CA 91360

Prof. Keiiti Aki  
Center for Earth Sciences  
University of Southern California  
University Park  
Los Angeles, CA 90089-0741

Prof. Shelton S. Alexander  
Geosciences Department  
403 Deike Building  
The Pennsylvania State University  
University Park, PA 16802

Dr. Kenneth Anderson  
BBNSTC  
Mail Stop 14/1B  
Cambridge, MA 02238

Dr. Ralph Archuleta  
Department of Geological Sciences  
University of California at Santa Barbara  
Santa Barbara, CA 93102

Dr. Thomas C. Bache, Jr.  
Science Applications Int'l Corp.  
10210 Campus Point Drive  
San Diego, CA 92121 (2 copies)

J. Barker  
Department of Geological Sciences  
State University of New York  
at Binghamton  
Vestal, NY 13901

Dr. T.J. Bennett  
S-CUBED  
A Division of Maxwell Laboratory  
11800 Sunrise Valley Drive, Suite 1212  
Reston, VA 22091

Mr. William J. Best  
907 Westwood Drive  
Vienna, VA 22180

Dr. N. Biswas  
Geophysical Institute  
University of Alaska  
Fairbanks, AK 99701

Dr. G.A. Bollinger  
Department of Geological Sciences  
Virginia Polytechnical Institute  
21044 Derring Hall  
Blacksburg, VA 24061

Dr. Stephen Bratt  
Science Applications Int'l Corp.  
10210 Campus Point Drive  
San Diego, CA 92121

Michael Browne  
Teledyne Geotech  
3401 Shiloh Road  
Garland, TX 75041

Mr. Roy Burger  
1221 Serry Road  
Schenectady, NY 12309

Dr. Robert Burrige  
Schlumberger-Doll Research Center  
Old Quarry Road  
Ridgefield, CT 06877

Dr. Jerry Carter  
Rondout Associates  
P.O. Box 224  
Stone Ridge, NY 12484

Dr. W. Winston Chan  
Teledyne Geotech  
314 Montgomery Street  
Alexandria, VA 22314-1581

Dr. Theodore Cherry  
Science Horizons, Inc.  
710 Encinitas Blvd., Suite 200  
Encinitas, CA 92024 (2 copies)

Prof. Jon F. Claerbout  
Department of Geophysics  
Stanford University  
Stanford, CA 94305

Prof. Robert W. Clayton  
Seismological Laboratory  
Division of Geological & Planetary Sciences  
California Institute of Technology  
Pasadena, CA 91125

Prof. F. A. Dahlen  
Geological and Geophysical Sciences  
Princeton University  
Princeton, NJ 08544-0636

Dr. Jeffrey W. Given  
Sierra Geophysics  
11255 Kirkland Way  
Kirkland, WA 98033

Prof. Anton W. Dainty  
Earth Resources Lab  
Massachusetts Institute of Technology  
42 Carleton Street  
Cambridge, MA 02142

Prof. Stephen Grand  
University of Texas at Austin  
Department of Geological Sciences  
Austin, TX 78713-7909

Prof. Adam Dziewonski  
Hoffman Laboratory  
Harvard University  
20 Oxford St  
Cambridge, MA 02138

Prof. Roy Greenfield  
Geosciences Department  
403 Deike Building  
The Pennsylvania State University  
University Park, PA 16802

Prof. John Ebel  
Department of Geology & Geophysics  
Boston College  
Chestnut Hill, MA 02167

Dan N. Hagedorn  
Battelle  
Pacific Northwest Laboratories  
Battelle Boulevard  
Richland, WA 99352

Eric Fielding  
SNEE Hall  
INSTOC  
Cornell University  
Ithaca, NY 14853

Kevin Hutchenson  
Department of Earth Sciences  
St. Louis University  
3507 Laclede  
St. Louis, MO 63103

Prof. Donald Forsyth  
Department of Geological Sciences  
Brown University  
Providence, RI 02912

Prof. Thomas H. Jordan  
Department of Earth, Atmospheric  
and Planetary Sciences  
Massachusetts Institute of Technology  
Cambridge, MA 02139

Prof. Art Frankel  
Mail Stop 922  
Geological Survey  
790 National Center  
Reston, VA 22092

Robert C. Kemerait  
ENSCO, Inc.  
445 Pineda Court  
Melbourne, FL 32940

Dr. Anthony Gangi  
Texas A&M University  
Department of Geophysics  
College Station, TX 77843

William Kikendall  
Teledyne Geotech  
3401 Shiloh Road  
Garland, TX 75041

Dr. Freeman Gilbert  
Inst. of Geophysics & Planetary Physics  
University of California, San Diego  
P.O. Box 109  
La Jolla, CA 92037

Prof. Leon Knopoff  
University of California  
Institute of Geophysics & Planetary Physics  
Los Angeles, CA 90024

Mr. Edward Giller  
Pacific Sierra Research Corp.  
1401 Wilson Boulevard  
Arlington, VA 22209

Prof. L. Timothy Long  
School of Geophysical Sciences  
Georgia Institute of Technology  
Atlanta, GA 30332



Prof. Art McGarr  
Mail Stop 977  
Geological Survey  
345 Middlefield Rd.  
Menlo Park, CA 94025

Dr. George Mellman  
Sierra Geophysics  
11255 Kirkland Way  
Kirkland, WA 98033

Prof. John Nabelek  
College of Oceanography  
Oregon State University  
Corvallis, OR 97331

Prof. Geza Nagy  
University of California, San Diego  
Department of Ames, M.S. B-010  
La Jolla, CA 92093

Prof. Amos Nur  
Department of Geophysics  
Stanford University  
Stanford, CA 94305

Prof. Jack Oliver  
Department of Geology  
Cornell University  
Ithaca, NY 14850

Prof. Robert Phinney  
Geological & Geophysical Sciences  
Princeton University  
Princeton, NJ 08544-0636

Dr. Paul Pomeroy  
Rondout Associates  
P.O. Box 224  
Stone Ridge, NY 12484

Dr. Jay Pulli  
RADIX System, Inc.  
2 Taft Court, Suite 203  
Rockville, MD 20850

Dr. Norton Rimer  
S-CUBED  
A Division of Maxwell Laboratory  
P.O. Box 1620  
La Jolla, CA 92038-1620

Prof. Larry J. Ruff  
Department of Geological Sciences  
1006 C.C. Little Building  
University of Michigan  
Ann Arbor, MI 48109-1063

Dr. Richard Sailor  
TASC Inc.  
55 Walkers Brook Drive  
Reading, MA 01867

Thomas J. Sereno, Jr.  
Science Application Int'l Corp.  
10210 Campus Point Drive  
San Diego, CA 92121

John Sherwin  
Teledyne Geotech  
3401 Shiloh Road  
Garland, TX 75041

Prof. Robert Smith  
Department of Geophysics  
University of Utah  
1400 East 2nd South  
Salt Lake City, UT 84112

Prof. S. W. Smith  
Geophysics Program  
University of Washington  
Seattle, WA 98195

Dr. Stewart Smith  
IRIS Inc.  
1616 North Fort Myer Drive  
Suite 1440  
Arlington, VA 22209

Dr. George Sutton  
Rondout Associates  
P.O. Box 224  
Stone Ridge, NY 12484

Prof. L. Sykes  
Lamont-Doherty Geological Observatory  
of Columbia University  
Palisades, NY 10964

Prof. Pradeep Talwani  
Department of Geological Sciences  
University of South Carolina  
Columbia, SC 29208

Prof. Ta-liang Teng  
Center for Earth Sciences  
University of Southern California  
University Park  
Los Angeles, CA 90089-0741

- Dr. R.B. Tittmann  
Rockwell International Science Center  
1049 Camino Dos Rios  
, P.O. Box 1085  
Thousand Oaks, CA 91360

Dr. Gregory van der Vink  
IRIS, Inc.  
1616 North Fort Myer Drive  
Suite 1440  
Arlington, VA 22209

William R. Walter  
Seismological Laboratory  
University of Nevada  
Reno, NV 89557

Dr. Gregory Wojcik  
Weidlinger Associates  
4410 El Camino Real  
Suite 110  
Los Altos, CA 94022

Prof. John H. Woodhouse  
Hoffman Laboratory  
Harvard University  
20 Oxford Street  
Cambridge, MA 02138

Dr. Gregory B. Young  
ENSCO, Inc.  
5400 Port Royal Road  
Springfield, VA 22151-2388

• Dr. Cliff Frolich  
Institute of Geophysics  
8701 North Mopac  
Austin, TX 78759

•

GOVERNMENT

Dr. Ralph Alewine III  
DARPA/NMRO  
1400 Wilson Boulevard  
Arlington, VA 01731-5000

Paul Johnson  
ESS-4, Mail Stop J979  
Los Alamos National Laboratory  
Los Alamos, NM 87545

Mr. James C. Battis  
GL/LWH  
Hanscom AFB, MA 22209-2308

Janet Johnston  
GL/LWH  
Hanscom AFB, MA 01731-5000

Dr. Robert Blandford  
DARPA/NMRO  
1400 Wilson Boulevard  
Arlington, VA 87185

Dr. Katharine Kadinsky-Cade  
GL/LWH  
Hanscom AFB, MA 01731-5000

Eric Chael  
Division 9241  
Sandia Laboratory  
Albuquerque, NM 01731-5000

Ms. Ann Kerr  
IGPP, A-025  
Scripps Institute of Oceanography  
University of California, San Diego  
La Jolla, CA 92093

Dr. John J. Cipar  
GL/LWH  
Hanscom AFB, MA 01731-5000

Dr. Max Koontz  
US Dept of Energy/DP 5  
Forrestal Building  
1000 Independence Avenue  
Washington, DC 20585

Mr. Jeff Duncan  
Office of Congressman Markey  
2133 Rayburn House Bldg.  
Washington, D.C. 20515

Dr. W.H.K. Lee  
Office of Earthquakes, Volcanoes,  
& Engineering  
345 Middlefield Road  
Menlo Park, CA 94025

Dr. Jack Evernden  
USGS - Earthquake Studies  
345 Middlefield Road  
Menlo Park, CA 94025

Dr. William Leith  
U.S. Geological Survey  
Mail Stop 928  
Reston, VA 22092

Art Frankel  
USGS  
922 National Center  
Reston, VA 22092

Dr. Richard Lewis  
Director, Earthquake Engineering & Geophysics  
U.S. Army Corps of Engineers  
Box 631  
Vicksburg, MS 39180

Dr. T. Hanks  
USGS  
Nat'l Earthquake Research Center  
345 Middlefield Road  
Menlo Park, CA 94025

James F. Lewkowicz  
GL/LWH  
Hanscom AFB, MA 01731-5000

Dr. James Hannon  
Lawrence Livermore Nat'l Laboratory  
P.O. Box 808  
Livermore, CA 94550

Mr. Alfred Lieberman  
ACDA/VI-OA State Department Bldg  
Room 5726  
320 - 21st Street, NW  
Washington, DC 20451

Stephen Mangino  
GL/LWH  
Hanscom AFB, MA 01731-5000

Dr. Frank F. Pilotte  
HQ AFTAC/TT  
Patrick AFB, FL 32925-6001

Dr. Robert Masse  
Box 25046, Mail Stop 967  
Denver Federal Center  
Denver, CO 80225

Katie Poley  
CIA-OSWR/NED  
Washington, DC 20505

Art McGarr  
U.S. Geological Survey, MS-977  
345 Middlefield Road  
Menlo Park, CA 94025

Mr. Jack Rachlin  
U.S. Geological Survey  
Geology, Rm 3 C136  
Mail Stop 928 National Center  
Reston, VA 22092

Richard Morrow  
ACDA/VI, Room 5741  
320 21st Street N.W  
Washington, DC 20451

Dr. Robert Reinke  
WL/NTESG  
Kirtland AFB, NM 87117-6008

Dr. Keith K. Nakanishi  
Lawrence Livermore National Laboratory  
P.O. Box 808, L-205  
Livermore, CA 94550

Dr. Byron Ristvet  
HQ DNA, Nevada Operations Office  
Attn: NVCG  
P.O. Box 98539  
Las Vegas, NV 89193

Dr. Carl Newton  
Los Alamos National Laboratory  
P.O. Box 1663  
Mail Stop C335, Group ESS-3  
Los Alamos, NM 87545

Dr. George Rothe  
HQ AFTAC/TGR  
Patrick AFB, FL 32925-6001

Dr. Kenneth H. Olsen  
Los Alamos Scientific Laboratory  
P.O. Box 1663  
Mail Stop C335, Group ESS-3  
Los Alamos, NM 87545

Dr. Michael Shore  
Defense Nuclear Agency/SPSS  
6801 Telegraph Road  
Alexandria, VA 22310

Howard J. Patton  
Lawrence Livermore National Laboratory  
P.O. Box 808, L-205  
Livermore, CA 94550

Donald L. Springer  
Lawrence Livermore National Laboratory  
P.O. Box 808, L-205  
Livermore, CA 94550

Mr. Chris Paine  
Office of Senator Kennedy, SR 315

Dr. Lawrence Turnbull  
OSWR/NED  
Central Intelligence Agency, Room 5G48  
Washington, DC 20505

United States Senate  
Washington, DC 20510

Colonel Jerry J. Perrizo  
AFOSR/NP, Building 410  
Bolling AFB  
Washington, DC 20332-6448

Dr. Thomas Weaver  
Los Alamos National Laboratory  
P.O. Box 1663, Mail Stop C335  
Los Alamos, NM 87545

J.J. Zucca  
Lawrence Livermore National Laboratory  
Box 808  
Livermore, CA 94550

Defense Technical Information Center  
Cameron Station  
Alexandria, VA 22314 (5 copies)

GL/SULL  
Research Library  
Hanscom AFB, MA 01731-5000 (2 copies)

Defense Intelligence Agency  
Directorate for Scientific &  
Technical Intelligence  
Washington, DC 20301

Secretary of the Air Force (SAFRD)  
Washington, DC 20330

AFTAC/CA  
(STINFO)  
Patrick AFB, FL 32925-6001

Office of the Secretary Defense  
DDR & E  
Washington, DC 20330

TACTEC  
Battelle Memorial Institute  
505 King Avenue  
Columbus, OH 43201 (Final Report Only)

HQ DNA  
Attn: Technical Library  
Washington, DC 20305

Mr. Charles L. Taylor  
GL/LWH

Hanscom AFB, MA 01731-5000

DARPA/RMO/RETRIEVAL  
1400 Wilson Boulevard  
Arlington, VA 22209

DARPA/RMO/Security Office  
1400 Wilson Boulevard  
Arlington, VA 22209

Geophysics Laboratory  
Attn: XO  
Hanscom AFB, MA 01731-5000

Geophysics Laboratory  
Attn: LW  
Hanscom AFB, MA 01731-5000

DARPA/PM  
1400 Wilson Boulevard  
Arlington, VA 22209

CONTRACTORS (Foreign)

Dr. Ramon Cabre, S.J.  
Observatorio San Calixto  
Casilla 5939  
La Paz, Bolivia

Prof. Hans-Peter Harjes  
Institute for Geophysik  
Ruhr University/Bochum  
P.O. Box 102148  
4630 Bochum 1, FRG

Prof. Eystein Husebye  
NTNF/NORSAR  
P.O. Box 51  
N-2007 Kjeller, NORWAY

Prof. Brian L.N. Kennett  
Research School of Earth Sciences  
Institute of Advanced Studies  
G.P.O. Box 4  
Canberra 2601, AUSTRALIA

Dr. Bernard Massinon  
Societe Radiomana  
27 rue Claude Bernard  
75005 Paris, FRANCE (2 Copies)

Dr. Pierre Mecheler  
Societe Radiomana  
27 rue Claude Bernard  
75005 Paris, FRANCE

Dr. Svein Mykkeltveit  
NTNF/NORSAR  
P.O. Box 51  
N-2007 Kjeller, NORWAY

FOREIGN (Others)

Dr. Peter Basham  
Earth Physics Branch  
Geological Survey of Canada  
1 Observatory Crescent  
Ottawa, Ontario, CANADA K1A 0Y3

Dr. Eduard Berg  
Institute of Geophysics  
University of Hawaii  
Honolulu, HI 96822

Dr. Michel Bouchon  
I.R.I.G.M.-B.P. 68  
38402 St. Martin D'Herès  
Cedex, FRANCE

Dr. Hilmar Bungum  
NTNF/NORSAR  
P.O. Box 51  
N-2007 Kjeller, NORWAY

Dr. Michel Campillo  
Observatoire de Grenoble  
I.R.I.G.M.-B.P. 53  
38041 Grenoble, FRANCE

Dr. Kin Yip Chun  
Geophysics Division  
Physics Department  
University of Toronto  
Ontario, CANADA M5S 1A7

Dr. Alan Douglas  
Ministry of Defense  
Blacknest, Brimpton  
Reading RG7-4RS, UNITED KINGDOM

Dr. Roger Hansen  
NTNF/NORSAR  
P.O. Box 51  
N-2007 Kjeller, NORWAY

Dr. Manfred Henger  
Federal Institute for Geosciences & Nat'l Res.  
Postfach 510153  
D-3000 Hanover 51, FRG

Ms. Eva Johannisson  
Senior Research Officer  
National Defense Research Inst.  
P.O. Box 27322  
S-102 54 Stockholm, SWEDEN

Dr. Fekadu Kebede  
Seismological Section  
Box 12019  
S-750 Uppsala, SWEDEN

Dr. Tormod Kvaerna  
NTNF/NORSAR  
P.O. Box 51  
N-2007 Kjeller, NORWAY

Dr. Peter Marshal  
Procurement Executive  
Ministry of Defense  
Blacknest, Brimpton  
Reading FG7-4RS, UNITED KINGDOM

Prof. Ari Ben-Menahem  
Department of Applied Mathematics  
Weizman Institute of Science  
Rehovot, ISRAEL 951729

Dr. Robert North  
Geophysics Division  
Geological Survey of Canada  
1 Observatory Crescent  
Ottawa, Ontario, CANADA K1A 0Y3

Dr. Frode Ringdal  
NTNF/NORSAR  
P.O. Box 51  
N-2007 Kjeller, NORWAY

Dr. Jorg Schlittenhardt  
Federal Institute for Geosciences & Nat'l Res.  
Postfach 510153  
D-3000 Hannover 51, FEDERAL REPUBLIC OF  
GERMANY

Prof. Daniel Walker  
University of Hawaii  
Institute of Geophysics  
Honolulu, HI 96822